BMC Biology

RESEARCH

Open Access

Melanin deposition and key molecular features in *Xenopus tropicalis* oocytes

Hongyang Yi[1,2†], Weizheng Liang[3†], Sumei Yang[1†], Han Liu[1], Jiayu Deng[1], Shuhong Han[1], Xiaohui Feng[4], Wenjie Cheng[5], Yonglong Chen[2*], Jing Hang[6*], Hongzhou Lu[1*] and Rensen Ran[2,6*]

Abstract

Background Melanin pigmentation in oocytes is a critical feature for both the esthetic and developmental aspects of oocytes, influencing their polarity and overall development. Despite substantial knowledge of melanogenesis in melanocytes and retinal pigment epithelium cells, the molecular mechanisms underlying oocyte melanogenesis remain largely unknown.

Results Here, we compare the oocytes of wild-type, $tyr^{-/-}$ and $mitf^{-/-}$ *Xenopus tropicalis* and found that $mitf^{-/-}$ oocytes exhibit normal melanin deposition at the animal pole, whereas $tyr^{-/-}$ oocytes show no melanin deposition at this site. Transmission electron microscopy confirmed that melanogenesis in $mitf^{-/-}$ oocytes proceeds normally, similar to wild-type oocytes. Transcriptomic analysis revealed that $mitf^{-/-}$ oocytes still express melanogenesis-related genes, enabling them to complete melanogenesis. Additionally, in *Xenopus tropicalis* oocytes, the expression of the MiT subfamily factor *tfe3* is relatively high, while *tfeb*, *mitf*, and *tfec* levels are extremely low. The expression pattern of *tfe3* is similar to that of *tyr* and other melanogenesis-related genes. Thus, melanogenesis in *Xenopus tropicalis* oocytes is independent of Mitf and may be regulated by other MiT subfamily factors such as Tfe3, which control the expression of genes like *tyr*, *dct*, and *tyrp1*. Furthermore, transcriptomic data revealed that changes in the expression of genes related to mitochondrial cloud formation represent the most significant molecular changes during oocyte development.

Conclusions Overall, these findings suggest that further elucidation of Tyr-dependent and Mitf-independent mechanisms of melanin deposition at the animal pole will enhance our understanding of melanogenesis and Oogenesis.

Keywords Oogenesis, Melanogenesis, *Xenopus tropicalis*, Mitochondrial cloud

†Hongyang Yi, Weizheng Liang and Sumei Yang contributed equally to this work.

*Correspondence:
Yonglong Chen
chenyl@sustech.edu.cn
Jing Hang
hangjbysy@163.com
Hongzhou Lu
luhongzhou@fudan.edu.cn
Rensen Ran
sankeshumy@163.com
[1] National Clinical Research Centre for Infectious Diseases, the Third People'S Hospital of Shenzhenand, the Second Affiliated Hospital of Southern University of Science and Technologyaq, Shenzhen 518112, China
[2] Department of Biology, School of Life Sciences, Southern University of Science and Technology, Shenzhen 518055, China
[3] Hebei Provincial Key Laboratory of Systems Biology and Gene Regulation, Central Laboratory, The First Affiliated Hospital of Hebei North University, Zhangjiakou, Hebei 075000, China
[4] Department of Obstetrics and Gynecology, The Fifth Affiliated Hospital of Sun Yat-Sen University, Zhuhai 519000, China
[5] Department of Urology, The Fifth Affiliated Hospital of Sun Yat-Sen University, Zhuhai 519000, China
[6] State Key Laboratory of Female Fertility Promotion, Center for Reproductive Medicine, Department of Obstetrics and Gynecology, Peking University Third Hospital, Beijing, China

Background

Oogenesis, the process by which oocytes (egg cells) develop, involves complex interactions among genetic, biochemical, and environmental factors [1]. In some species, oocytes undergo melanin deposition during this process. Melanin pigmentation in oocytes is a critical feature that affects not only the esthetic attributes of the eggs but also their survival and fitness in natural environments [2–5]. For instance, melanin pigmentation can protect the developing oocyte from UV (ultraviolet) radiation and oxidative stress, thereby contributing to the overall viability of the embryo [6, 7]. Additionally, melanin pigment granules may play a role in the thermal regulation of the eggs, influencing embryonic development rates [8]. Therefore, understanding the molecular mechanisms governing melanin synthesis in oocytes provides insights into oocyte development and other broader biological phenomena, such as gene regulatory networks, organelle biogenesis, cellular differentiation, and intracellular transport.

In vertebrates, melanogenesis primarily occurs in melanocytes, the retinal pigment epithelium (RPE), and the oocytes of certain species [9, 10]. The melanogenesis process involves a series of enzymatic reactions that begin with the amino acid tyrosine [11, 12]. Central to melanogenesis is the enzyme tyrosinase, which catalyzes the initial and rate-limiting steps of melanin synthesis, converting tyrosine into dihydroxyphenylalanine (DOPA) and subsequently into dopaquinone [9, 11–13]. Further complex biochemical transformations lead to the production of different types of melanin, mainly eumelanin (brown to black pigment) and pheomelanin (yellow to red pigment) [11]. The type and amount of melanin produced are regulated by genetic, hormonal, and environmental factors, making melanogenesis a highly dynamic and tightly controlled process.

The molecular regulation of melanogenesis is predominantly controlled by the microphthalmia-associated transcription factor (MITF), a master regulator in melanocytes that governs the expression of essential melanogenic enzymes and structural proteins [11, 12, 14]. MITF specifically regulates enzymes such as tyrosinase, tyrosinase-related protein 1 (TRP-1), and tyrosinase-related protein 2 (TRP-2) [11, 14]. MITF activity is modulated by several signaling pathways, including cAMP/protein kinase A (PKA), Wnt/β-catenin, and mitogen-activated protein kinase (MAPK) [13, 14]. These pathways are activated by various extracellular signals, such as UV radiation, hormones, and cytokines, which collectively modulate MITF expression and activity, highlighting the complexity of melanin production regulation. Despite significant advances in understanding the molecular mechanisms of melanogenesis [14, 15], many aspects remain unclear. The roles of non-coding RNAs, epigenetic modifications, and genetic polymorphisms in melanogenic pathways are areas of ongoing research [16, 17].

It is noteworthy that although melanogenesis plays a crucial role in *Xenopus* oocyte development, the molecular regulatory mechanisms of *Xenopus* oocyte melanogenesis remain largely unknown [4, 5, 18–24]. Previous research has shown that tyrosinase activity is markedly higher in stage III and stage IV *Xenopus* oocytes compared to other stages [20, 24]. Additionally, studies have shown that while $a^p a^p$ *Xenopus laevis* oocytes lack pigmentation and contain no melanosomes, the tyrosinase activity in $a^p a^p$ *Xenopus laevis* oocytes is twice that of wild-type *Xenopus laevis* oocytes [22]. Numerous experiments have confirmed that the tyrosinase inhibitor PTU (1-phenyl 2-thiourea) can induce the production of melanin-free oocytes and tadpoles in *Xenopus* [5, 19, 24]. Furthermore, gene-editing technologies such as TALEN (transcription activator-like effector nuclease) and CRISPR/Cas9 (clustered regularly interspaced short palindromic repeats) have produced tyrosinase knockout lines of *Xenopus laevis* and *Xenopus tropicalis* [25, 26]. However, the molecular mechanisms regulating tyrosinase expression in oocytes remain unclear. Due to the significant differences between the intracellular and extracellular environments of oocytes and melanocytes [1, 15, 27, 28], the similarities and differences in the molecular regulatory mechanisms of melanogenesis in oocytes and melanocytes are still unknown.

In our previous research, we successfully established $mitf^{-/-}$ and $tyr^{-/-}$ *Xenopus tropicalis* lines using CRISPR/Cas9 gene editing technology [26]. We discovered that while $tyr^{-/-}$ *Xenopus tropicalis* oocytes completely lacked melanin deposition, $mitf^{-/-}$ *Xenopus tropicalis* oocytes exhibited normal melanin deposition [26]. This unexpected oocyte phenotype further motivated us to study the molecular regulatory mechanisms of oocyte melanogenesis in *Xenopus tropicalis*. Therefore, in this study, we utilized oocytes from three genotypes of *Xenopus tropicalis*: WT, $mitf^{-/-}$, and $tyr^{-/-}$, to investigate the molecular characteristics of oocyte melanogenesis. Our results revealed that although the core enzymes involved in *Xenopus tropicalis* oocyte melanogenesis are tyrosinase, Trp1, and Trp2, the master regulator of these core enzymes' expression is not Mitf. Thus, our findings suggest that *Xenopus tropicalis* oocyte melanogenesis depends on a master regulator other than Mitf, revising our understanding of the function of the *mitf* gene and highlighting the importance of further exploring the molecular regulatory mechanisms of oocyte melanogenesis.

Results

Disruption of the Mitf basic helix-loop-helix leucine zipper domain impairs its function

MITF, a member of the basic helix-loop-helix leucine zipper (bHLH-LZ) family, is highly conserved and serves as a pivotal regulator in numerous biological processes, including cellular differentiation, proliferation, and survival across various tissues [14, 29]. Initially identified for its role in ocular development, MITF has since emerged as a multifaceted transcription factor with implications extending far beyond its namesake. Its intricate involvement in melanocyte biology, osteoclastogenesis, and immune response underscores its versatile functionality [14, 30, 31]. Structurally, MITF exhibits a modular organization characterized by distinct domains responsible for DNA binding (the bHLH-LZ domain binds DNA as dimers), protein–protein interactions, and transcriptional activation (a strong transcription activation domain at the N-terminus and a much weaker second transactivation domain at the C-terminus) [14, 29]. These domains intricately cooperate to confer specificity in target gene recognition, recruitment of cofactors, and modulation of transcriptional activity [29]. When both transcription activation domains (TADs) of MITF are inactivated, the mutated MITF can form dimers with wild-type MITF, exerting a dominant negative effect [32]. Given that the bHLH-LZ domain is primarily responsible for the DNA-binding function of MITF, disrupting this domain results in the loss of MITF function [14, 29]. Therefore, we utilized CRISPR/Cas9 gene editing technology to disrupt the bHLH-LZ domain of Mitf in *Xenopus tropicalis* to achieve *mitf* gene knockout [26].

Generally, the transcription of the *MITF* gene locus mRNA in mammals is complex and variable (Additional file 1: Fig. S1). However, NCBI (National Center for Biotechnology Information) records show only one *mitf* transcript for *Xenopus tropicalis* and three *mitf* transcripts for zebrafish (Additional file 1: Fig. S2A). This discrepancy may be due to limited research on *mitf* mRNA transcription in these species. Analysis of *MITF* mRNA transcription in humans, mice, *Xenopus tropicalis*, and zebrafish reveals variability at the 5' end and consistency at the 3' end (Additional file 1: Fig. S1 and Fig. S2A). Within the same species, the final few exons encoding these isoforms are identical, resulting in all MITF protein isoforms having the same C-terminus, likely due to the presence of highly conserved bHLH-LZ and TAD domains in these regions [14, 29]. To disrupt all isoforms encoded by the *Xenopus tropicalis mitf* gene locus, we designed a Cas9-targeted knockout site on the penultimate exon (Fig. 1A and Figure S2.A-C). According to Alphafold predictions, the bHLH-LZ and TAD domains are highly conserved between *Xenopus tropicalis* Mitf and human MITF (Additional file 1: Fig. S2B-C). The DNA and polypeptide binding sites within the bHLH-LZ domain exhibit significant conservation across species, and our designed guide RNA targets these conserved sites (Additional file 1: Fig. S2D-E). This suggests that in *mitf*$^{-/-}$ *Xenopus tropicalis*, the core bHLH-LZ domain of *Mitf* isoforms is disrupted, impairing their function. Indeed, following CRISPR/Cas9 knockout of *mitf* in *Xenopus tropicalis*, the resulting *mitf*$^{-/-}$ frogs lack melanocytes, xanthophores, and granular glands (Fig. 1B–F) [26]. During vertebrate eye development, various Mitf isoforms play crucial regulatory roles. Studies on various Mitf mutant mouse strains demonstrate that mutations in the bHLH-LZ domain of mouse MITF lead to abnormal eye development, including smaller eyes and aberrant pigmentation [30]. In contrast, *mitf*$^{-/-}$ *Xenopus tropicalis* exhibit normal eye size with apparently normal eye pigmentation [26]. Given the complexity of MITF's regulatory role in eye development and the subtle nature of some phenotypic abnormalities [30], further research is needed to assess whether the retina and RPE development in *mitf*$^{-/-}$ *Xenopus tropicalis* are truly unaffected (Fig. 1F). Overall, these data suggest that in *mitf*$^{-/-}$ *Xenopus tropicalis*, the disruption of the core bHLH-LZ domain of Mitf impairs the critical regulatory functions of various Mitf isoforms, particularly in melanocyte development and melanogenesis.

Absence of melanogenesis in the skin of *mitf*$^{-/-}$ *Xenopus tropicalis*

To investigate the molecular changes in Mitf-regulated target gene expression in *mitf* knockout *Xenopus*

(See figure on next page.)

Fig. 1 The *mitf*$^{-/-}$Xenopus tropicalis. **A** The knockout site of *mitf* in *Xenopus tropicalis*. **B** The genotype of *mitf*$^{-/-}$ *Xenopus tropicalis* ($n=40$ tadpoles). **C** Dorsal and ventral views of representative wild-type (WT) and *mitf*$^{-/-}$ *Xenopus tropicalis* (WT, $n=10$ froglets; *mitf*$^{-/-}$, $n=10$ froglets). **D** Dorsal and ventral views of representative WT and *mitf*$^{-/-}$ *Xenopus tropicalis* at 1 year old (WT, $n=10$ frogs; *mitf*$^{-/-}$, $n=10$ frogs). **E** Hematoxylin and eosin staining of representative dorsal skin tissue sections from WT, *mitf*$^{-/-}$, and *mitf*$^{-/-}$ rescue (G0 generation after gene knockout site repair) *Xenopus tropicalis*. Three frogs of each genotype were examined. Tissue samples were embedded in paraffin and sectioned at 6 μm thickness, with at least 10 paraffin sections observed per frog. Black arrows indicate melanocytes. **F** Hematoxylin and eosin staining of representative eye tissue sections from WT and *mitf*$^{-/-}$ *Xenopus tropicalis*. Three frogs of each genotype were examined. Tissue samples were embedded in paraffin and sectioned at 6 μm thickness, with at least 10 paraffin sections observed per frog. Black arrows indicate the RPE, and red arrows indicate melanocytes in the choroid layer. DS, dorsal view; VS, ventral view. Scale bars: 5 mm in **C** and **D**, 50 μm in **E** and **F**

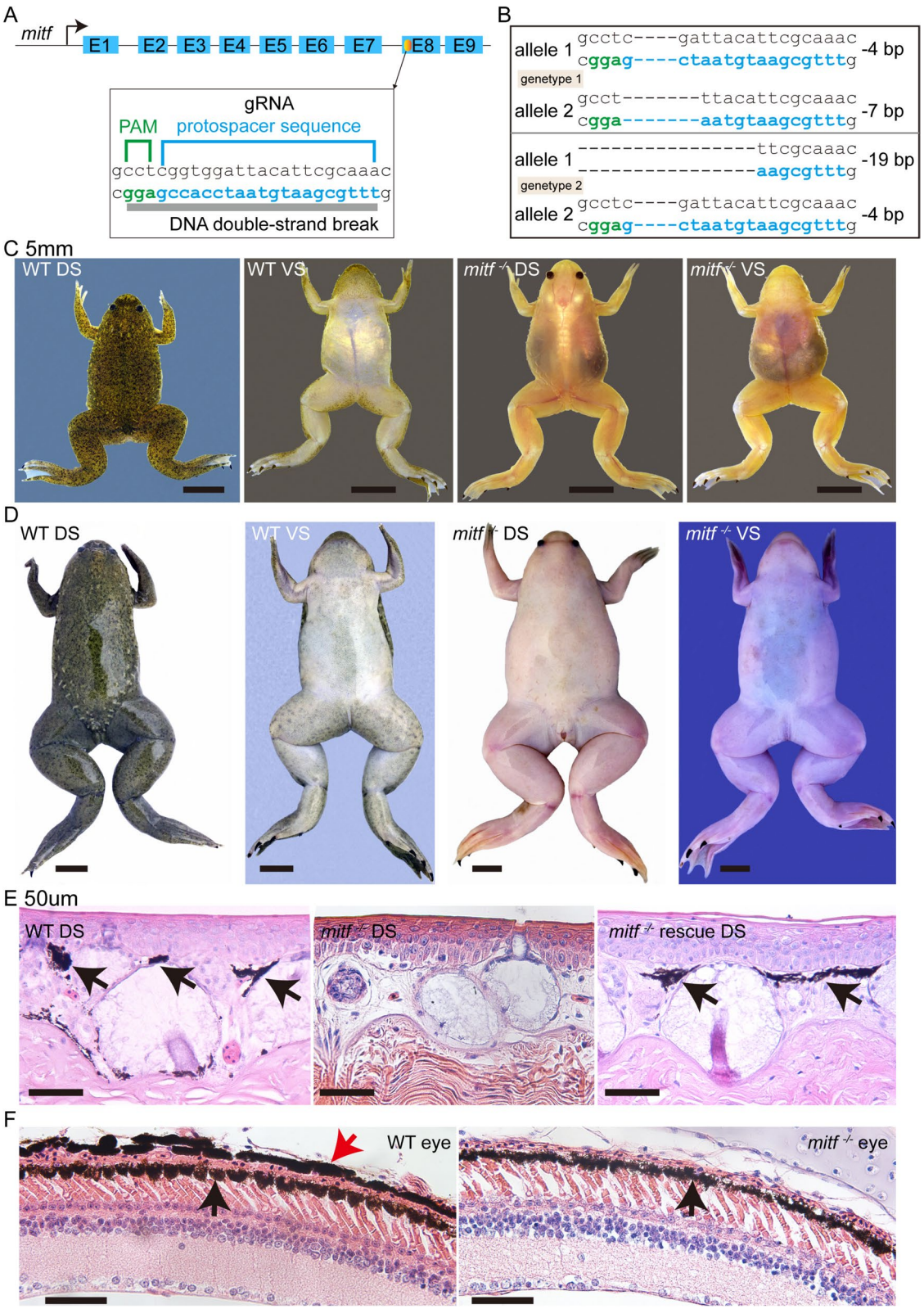

Fig. 1 (See legend on previous page.)

tropicalis, we performed Bulk RNA-seq on dorsal and ventral skin samples from adult wild-type (WT) and *mitf*$^{-/-}$ frogs. It is well-established that genes involved in melanogenic enzymes (e.g., *TYR*, *TYRP1*, *DCT*), melanosome ionic equilibrium (e.g., *SLC45A2*, *SLC24A5*), melanocyte development signaling pathways (e.g., *MC1R*), and melanosome biogenesis (e.g., *MLANA*, *PMEL*) are regulated by MITF (Fig. 2A). We first assessed the expression of these melanogenesis-related target genes. As expected, the expression levels of *tyr*, *tyrp1*, *dct*, *slc45a2*, *slc24a5*, *mc1r*, *mlana*, and *pmel* were significantly reduced in both dorsal and ventral skin samples of *mitf*$^{-/-}$ *Xenopus tropicalis* (Fig. 2B–C and Additional file 2: Table S1). In WT (wild-type) frogs, sequencing data confirms that the expression of melanin biosynthesis-related genes in the dorsal skin is higher than in the ventral skin (Additional file 1: Fig. S3). The apparent discrepancy in Fig. 2B and C arises from how we presented the data. Specifically, we normalized the expression data for both the dorsal and ventral skin, resulting in similar color representations for melanin-related gene expression in both regions. Additionally, melanocyte marker genes such as *slc24a5*, *ednrb2*, *kcnj13*, *trpm1*, and *mlph* also exhibited significantly reduced expression in the skin samples of *mitf*$^{-/-}$ frogs (Fig. 2B-C and Additional file 2: Table S1).We then examined the expression of these genes in eye samples from adult WT and *mitf*$^{-/-}$ *Xenopus tropicalis*. However, the expression of melanogenesis-related genes was not consistently reduced in the eyes of *mitf*$^{-/-}$ frogs (Additional file 2: Table S1). This discrepancy may be attributed to the presence of RPE cells in the retina, despite the absence of melanocytes in the choroid of *mitf*$^{-/-}$ *Xenopus tropicalis* eyes [26]. In mammals, MITF significantly influences the development of the RPE and retina by regulating the expression of genes such as *RDH5*, *RLBP1*, *MSI2*, *DAPL1*, miR204/211, *NF2*, *BEST1*, *PGC1α*, *PEDF* (*SERPINF1*), *PMEL*, *TYRP1*, and *TYR* [30]. However, in *mitf*$^{-/-}$ *Xenopus tropicalis* eyes, the expression levels of *rdh5*, *rlbp1*, *msi2*, *dapl1*, miR204/211, *nf2*, *best1*, *pgc1α*, and *pedf* did not show significant changes compared to wild-type eyes (Fig. 2D–K and Additional file 2: Table S2). Similarly, the expression of melanogenesis-related genes such as *pmel*, *tyrp1*, and *tyr*, which are regulated by MITF, were not significantly decreased in *mitf*$^{-/-}$ *Xenopus tropicalis* eyes (Additional file 1: Fig.S4 and Additional file 2: Table S2). Additionally, there was no significant difference in the expression of *rpe65*, a gene crucial for RPE cells, between wild-type and *mitf*$^{-/-}$ *Xenopus tropicalis* eyes (Additional file 1: Fig. S4 and Additional file 1: Table S2). These findings indicate that RPE cells in *mitf*$^{-/-}$ *Xenopus tropicalis* eyes can still develop into functional RPE cell layers despite the disruption of the Mitf bHLH-LZ domain [26]. However, the absence of melanocytes in the choroid layer of *mitf*$^{-/-}$ *Xenopus tropicalis* eyes confirms the lack of melanocyte development and melanogenesis [26]. In conclusion, this molecular evidence demonstrates that disrupting the Mitf bHLH-LZ domain in *Xenopus tropicalis* leads to a loss of Mitf activity, resulting in the absence of melanocytes and melanogenesis in the skin samples of *mitf*$^{-/-}$ *Xenopus tropicalis*, thereby contributing to their colorless and transparent appearance [26].

Normal oocyte melanin deposition in *mitf*$^{-/-}$ *Xenopus tropicalis* during oogenesis

In *mitf*$^{-/-}$ *Xenopus tropicalis*, the absence of melanocyte development in the skin led us to predict that oocytes in female *mitf*$^{-/-}$ *Xenopus tropicalis* would also lack melanin deposition [26]. However, contrary to our prediction, melanin deposition in *mitf*$^{-/-}$ *Xenopus tropicalis* oocytes was normal, with their pigmentation pattern being almost indistinguishable from that of wild-type oocytes (Fig. 3A–B) [26]. Additionally, the ovarian membrane of *mitf*$^{-/-}$ *Xenopus tropicalis*, which encases the ovaries, exhibited black spots similar to those observed in wild-type ovarian membranes (Fig. 3A–B). In contrast, *tyr*$^{-/-}$ *Xenopus tropicalis* lacked black spots on the ovarian membrane and showed no melanin deposition in their oocytes (Fig. 3C). Specifically, in a 24-mm^2 area of the ovarian membrane, the number of black spots in the WT group was 19.5, significantly higher than the 15.3 black spots in the mitf-/- group (P value = 0.0446) (Additional file 1: Fig.S5). TEM revealed that melanosomes formed normally in both wild-type and *mitf*$^{-/-}$ *Xenopus tropicalis* oocytes (Fig. 3D–G). Thus, the normal melanin deposition in mitf-/- *Xenopus tropicalis* oocytes indicates that disrupting the bHLH-LZ domain of Mitf does not affect melanogenesis in these oocytes. Conversely, the absence of melanin deposition in *tyr*$^{-/-}$ *Xenopus tropicalis* oocytes indicates that melanogenesis in *Xenopus tropicalis* oocytes depends on Tyr. Both WT and *mitf*$^{-/-}$ *Xenopus tropicalis* ovarian membranes exhibited black spots, while *tyr*$^{-/-}$ *Xenopus tropicalis* ovarian membranes did not (Fig. 3A–C). This suggests that the black spots on the ovarian membranes are likely caused by melanocytes and that melanin synthesis in these spots depends on Tyr. The black spots on the ovarian membranes of WT and *mitf*$^{-/-}$ *Xenopus tropicalis* contained numerous melanosomes, which are characteristic organelles of melanocytes, filled with abundant melanin granules (Fig. 3H–K). This indicates that the black spots on the ovarian membranes are primarily composed of melanocytes, resulting in their black coloration. Furthermore, this finding implies that the black spots on the ovarian membranes may represent the existence of a novel type of melanocyte whose

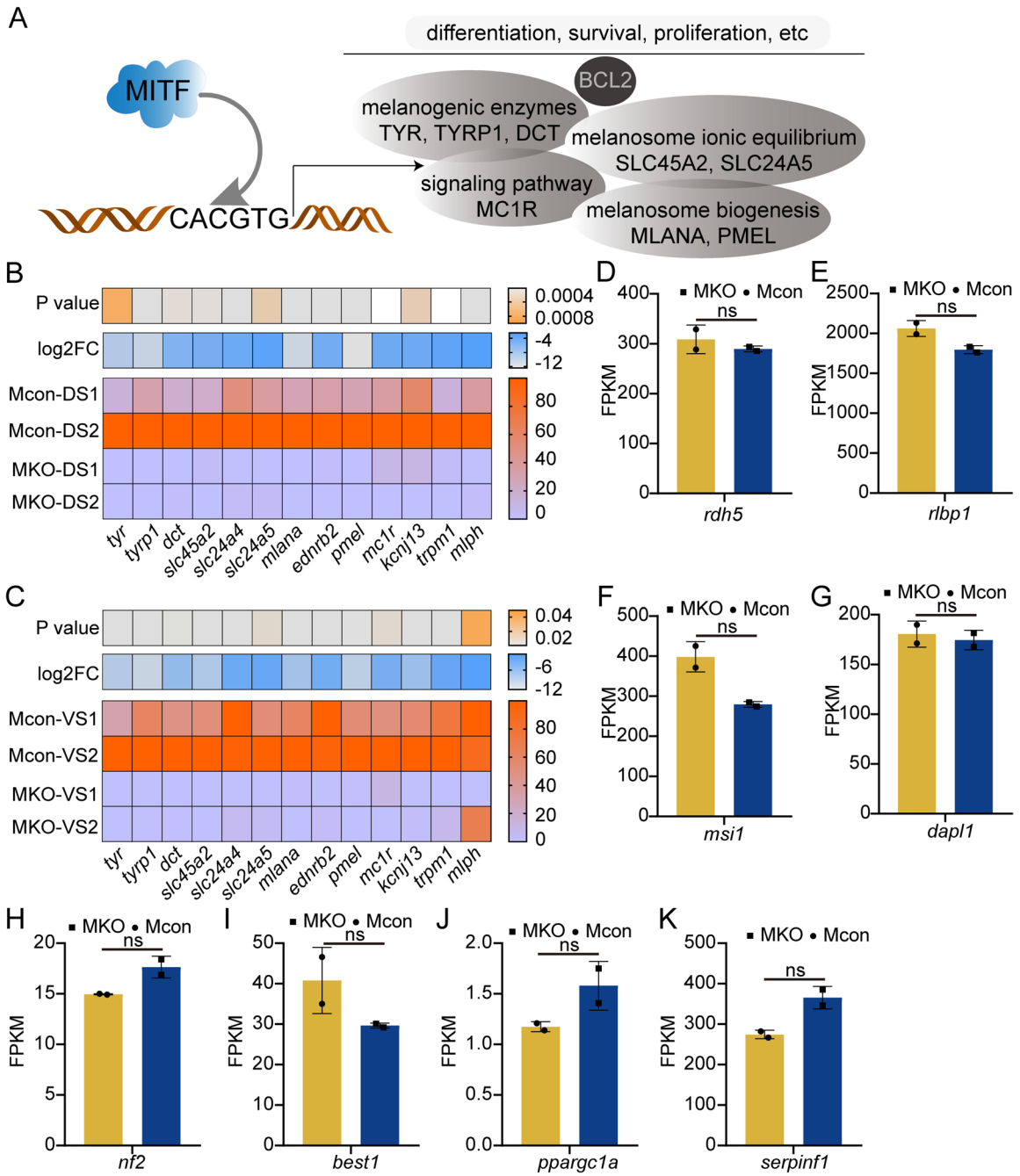

Fig. 2 *Xenopus tropicalis* Mitf regulates the expression of genes related to melanocyte development. **A** The cartoon provides a schematic representation of how the human MITF protein regulates the expression of target genes via the M-box (CACGTG), thereby controlling melanocyte development. **B**, **C** Heat maps show the differential expression of genes associated with melanocyte development in the dorsal (**B**) and ventral (**C**) skin of WT and *mitf*$^{-/-}$ *Xenopus tropicalis*. The FPKM values for each gene were normalized using the normalization function in GraphPad Prism 8.0 software, which was also used to create the heat maps. Mcon-DS1, Mcon-DS2, MKO-DS1, and MKO-DS2 represent two replicates of dorsal skin from WT and *mitf*$^{-/-}$ *Xenopus tropicalis*, respectively. Similarly, Mcon-VS1, Mcon-VS2, MKO-VS1, and MKO-VS2 represent two replicates of ventral skin from WT and *mitf*$^{-/-}$ *Xenopus tropicalis*, respectively. Each replicate sample from wild-type and *mitf*$^{-/-}$ *Xenopus tropicalis* was obtained from the dorsal or ventral skin of three frogs. **D–K** The expression of Mitf-activated target genes (*rdh5*, *rlbp1*, *msi1*, *dapl1*, *nf2*, *best1*, *ppargc1a*, *serpinf1*) in the eyes of WT and *mitf*$^{-/-}$ *Xenopus tropicalis* (unpaired *t* test)

development is not regulated by Mitf, warranting further investigation.

RNA-seq data indicated that *mitf* mRNA expression levels were low in both WT and *mitf*$^{-/-}$ *Xenopus tropicalis* during oogenesis, with no statistically significant differences observed despite a decreasing trend as oocyte development progressed (Fig. 3L). The expression levels of *tyr* mRNA showed no significant differences between WT and *mitf*$^{-/-}$ *Xenopus tropicalis* during oogenesis. In both, *tyr* mRNA expression significantly decreased as oocyte development proceeded. Specifically, *tyr* mRNA levels remained stable until stage 3, then markedly decreased at stage 4, continuing to very low levels by stage 6 (Fig. 3M). This pattern of *tyr* mRNA expression is consistent with previous reports on *Xenopus laevis* oogenesis [22, 33–35]. The expression levels of *tyrp1* and *dct* mRNA followed similar patterns to that of *tyr* mRNA (Additional file 1: Figure S6). These findings suggest that the expression of key melanogenic enzymes peaks at stage 3 during *Xenopus tropicalis* oogenesis and then gradually decreases, with *tyr* mRNA expression reaching very low levels after oocyte maturation.

Who regulates the expression of *tyr* mRNA during oocyte melanogenesis? In melanocytes, melanogenesis is primarily controlled by MITF, which regulates key enzymes such as TYR and TYRP1 [14]. However, during oocyte development in *Xenopus tropicalis*, *mitf* mRNA levels are low, and normal melanogenesis occurs in *mitf*$^{-/-}$ oocytes despite targeting and disrupting the core bHLH-LZ domain (Fig. 3A–G) [26]. This suggests that Mitf is not the master regulator of oocyte melanogenesis in *Xenopus tropicalis*. In vertebrates, the MiT subfamily of transcription factors, including TFEB, TFE3, and TFEC, can form heterodimers with MITF and bind to E-box sequences (typically a 6-bp CANNTG motif) in the promoter regions of target genes like *TYR*, *DCT*, *TYRP1*, and *PMEL* [14]. This raises the question: do TFEB, TFEC, or TFE3 directly regulate the expression of key enzymes such as Tyr, Dct, and Tryp1 in *mitf*$^{-/-}$ *Xenopus tropicalis* oocytes, or do they compensate for the loss of MITF to ensure normal melanogenesis? During oogenesis in both WT and *mitf*$^{-/-}$ *Xenopus tropicalis*, *tfeb* and *tfec* mRNA levels were low, whereas *tfe3* mRNA levels were relatively high and showed a similar trend to *tyr*, *tyrp1*, and *dct* mRNA (Fig. 3N–O and Additional file 1: Fig. S6A-C). There were no significant differences in *tfe3* mRNA expression between WT and *mitf*$^{-/-}$ oocytes (Fig. 3N). Additionally, the amino acid sequences of TFE3 and MITF are largely identical (Additional file 1: Fig.S6D). We hypothesize that during oocyte development in *Xenopus tropicalis*, melanin deposition in the animal pole of oocytes may be regulated by one or more members of the MiT subfamily (MITF, TFEB, TFE3, and TFEC). These factors might control the expression of genes such as *tyr*, *dct*, and *tyrp1* as needed to facilitate melanogenesis (UM2 in Fig. 3P). Alternatively, the MiT subfamily may regulate the transcription of these genes into mRNA, which is then stored as maternal RNA in oocytes and degraded or translated as necessary to complete melanogenesis (UM1 in Fig. 3P).

Next, we used JASPAR [36] to predict Tfe3's regulation of pigment synthesis genes *tyr* and *dct*. Results indicate that transcription factors in the MiT family (Mitf, Tfe3, Tfeb, Tfec) share a common DNA-binding motif, CAC GTGAC (Additional file 1: Fig.S7). Using NCBI data, we selected the 2000 bp upstream of the transcription start site (TSS) as the promoter regions of these target genes. JASPAR analysis revealed that Tfe3 has more binding sites in the tyr and dct promoters compared to Mitf (Fig. 4A–C and Additional file 3: Supplementary Note), suggesting that Tfe3 regulates their expression. Dual-luciferase assays confirmed this hypothesis, showing that Tfe3 regulates *tyr* and *dct* expression (Fig. 4D–E). Additionally, in oocytes, *tfe3* mRNA is expressed at levels significantly higher than *mitf*, *tfeb*, and *tfec* mRNAs and is comparable to *tyr* mRNA, being hundreds to thousands of times higher than the others. These results indicate that Tfe3, translated from the abundant *tfe3* mRNA, likely regulates pigment deposition in oocytes.

(See figure on next page.)

Fig. 3 Tyr regulates melanin deposition in *Xenopus tropicalis* oocytes. **A–C** Representative images show the ovarian from 1-year-old WT, *mitf*$^{-/-}$, and *tyr*$^{-/-}$ female *Xenopus tropicalis*, with three frogs observed for each genotype ($n = 9$ frogs). In **A** and **B**, magnified views of black spots on the ovarian peritoneum, indicated by blue arrows in the upper panels, are shown in the corresponding lower panels and are also indicated by blue arrows. The scale bars in the upper panels of **A**, **B,** and **C** are 0.5 mm, and in the lower panels, they are 0.1 mm. **D**, **F** Figures present TEM images of oocytes from one-year-old WT and *mitf*$^{-/-}$ *Xenopus tropicalis*. **E** and **G** are enlarged views of the regions indicated by red arrows in **D** and **F**, respectively. **H, J** Figures display TEM images of black spots on the ovarian peritoneum of 1-year-old WT and *mitf*$^{-/-}$ *Xenopus tropicalis*. **I** and **K** are enlarged views of the regions indicated by red arrows in **H** and **J**, respectively. The scale bars are as shown in the images. All images in **D**–**K** are representative ($n = 3$ frogs). **L**–**O** Figures show the mRNA expression levels of *mitf*, *tyr*, *tfe3*, and *tfec* during oocyte development in WT and *mitf*$^{-/-}$ *Xenopus tropicalis*, presented as FPKM values. **P** The cartoon provides a schematic diagram summarizing the possible molecular mechanisms regulating melanin deposition in *Xenopus tropicalis* oocytes. For the *P* values of the data in **L–O**, please refer to Supplementary Table S3. The statistical tests are the Wald test and the Likelihood ratio test in Deseq2

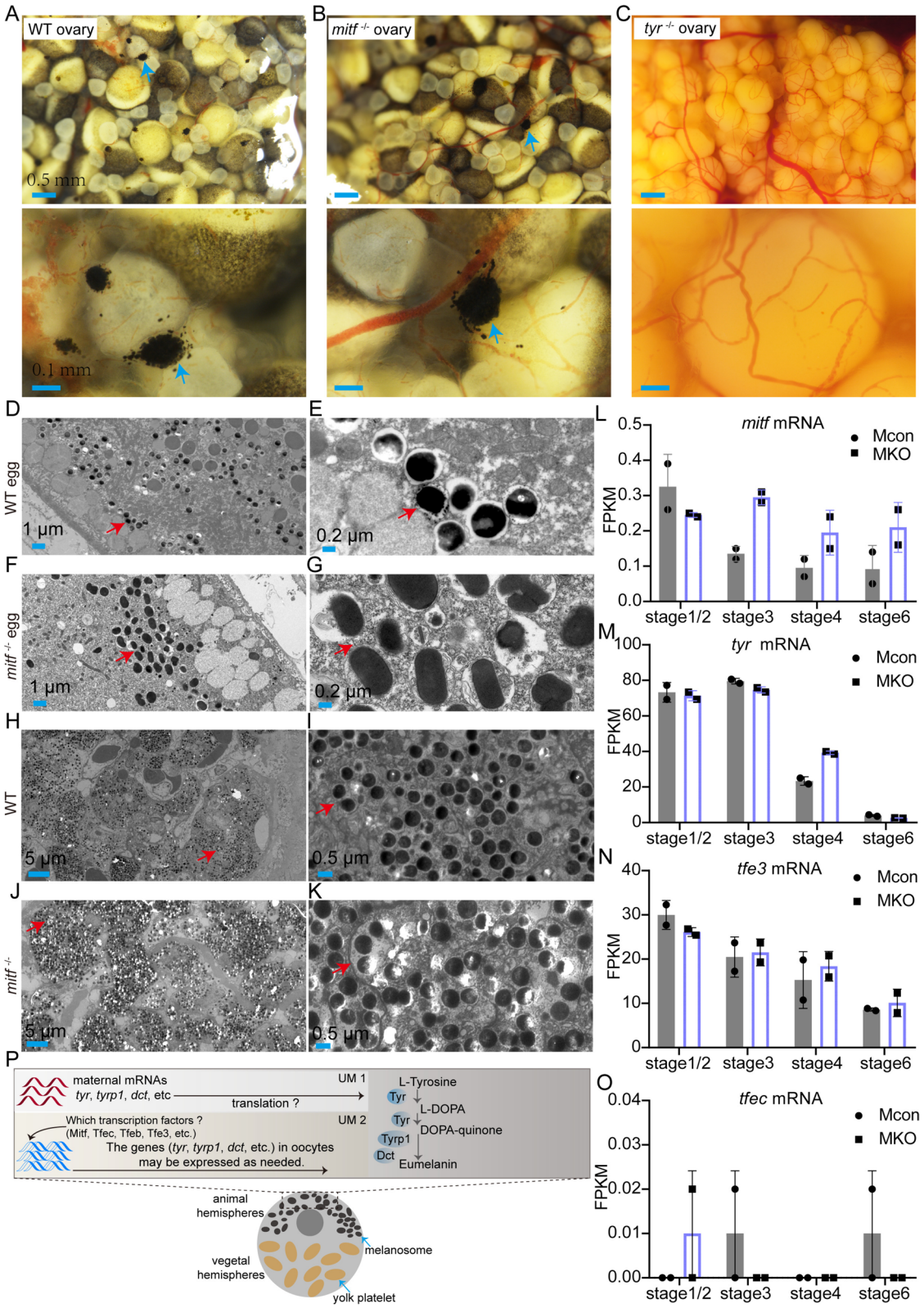

Fig. 3 (See legend on previous page.)

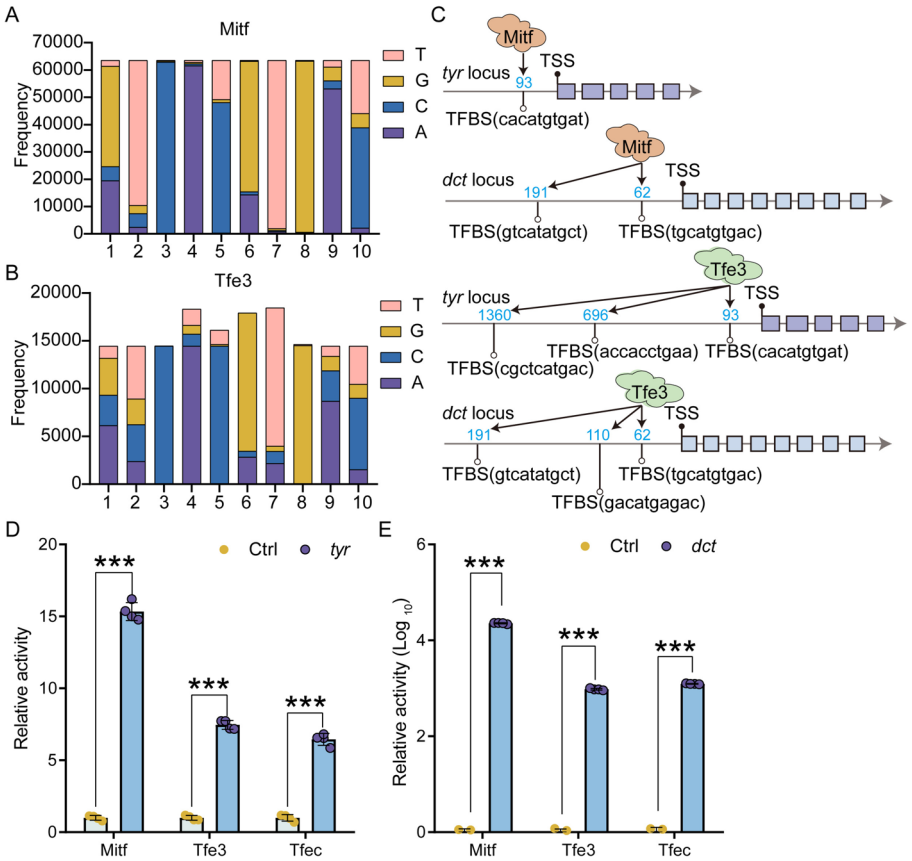

Fig. 4 MiT family transcription factors Tfe3, Mitf, and Tfec regulate the expression of the *tyr* and *dct* genes. **A–B** show the nucleotide frequency of different bases at various positions within the DNA binding motifs for Mitf and Tfe3. Data were obtained from JASPAR. **C** The DNA binding motifs for Mitf and Tfe3 in the promoter region of tyr and dct (2000 bp upstream of the transcription start site, TSS). The blue numbers indicate the distance (in base pairs) from the TSS. Data were obtained from JASPAR and NCBI. **D–E** Present dual-luciferase assay results for the regulation of *tyr* and *dct* expression by Mitf, Tfe3, and Tfec ($n=4$). *** indicates a P value < 0.001, as determined by an unpaired t test

Further examination of the mRNA expression of melanogenesis-related genes (*oca2*, *pmel*, *slc24a5*, *slc45a2*, *atp7a*, and *gpnmb*) revealed patterns similar to those of *tfe3* and *tyr* mRNA (Fig. 5A). Specifically, during stages 1 to 3 of oocyte development, these genes maintained relatively high expression levels, which significantly decreased during stages 4 to 6 (Fig. 5A). In contrast, the mRNA expression of genes involved in the synthesis of pterinosomes in xanthophores and guanine platelet crystals in iridophores did not exhibit the same pattern as *tfe3* and *tyr* mRNA (Fig. 5B–C). This suggests that the synthesis of pigments related to pterinosomes and guanine platelet crystals in *Xenopus tropicalis* oocytes is likely not regulated by Tfe3. The expression trend of melanogenesis-related genes in *Xenopus tropicalis* oocytes closely mirrored that of *tfe3* mRNA (Fig. 5A), indicating a potential regulatory role of Tfe3 in melanogenesis-related gene expression. However, further experimental validation is required. Overall, melanogenesis in *Xenopus tropicalis* oocytes appears to depend on Tyr rather than Mitf, challenging the previous understanding of Mitf as the master regulator of melanocyte development and melanogenesis and suggesting a different role for *mitf* in oocyte development.

(See figure on next page.)

Fig. 5 The expression of key genes involved in pigment synthesis progressively decreases during oocyte development in *Xenopus tropicalis*. **A** During oocyte development in WT and *mitf*$^{-/-}$ *Xenopus tropicalis*, the mRNA expression levels of genes associated with melanin synthesis pathways are shown as FPKM values. **B**, **C** During oocyte development in WT and *mitf*$^{-/-}$ *Xenopus tropicalis*, the mRNA expression levels of genes associated with carotenoid and pteridine synthesis pathways are shown as FPKM values. For the P values of the data in figures, please refer to Additional file 2: Table S3. The statistical tests are the Wald test and the Likelihood ratio test in Deseq2

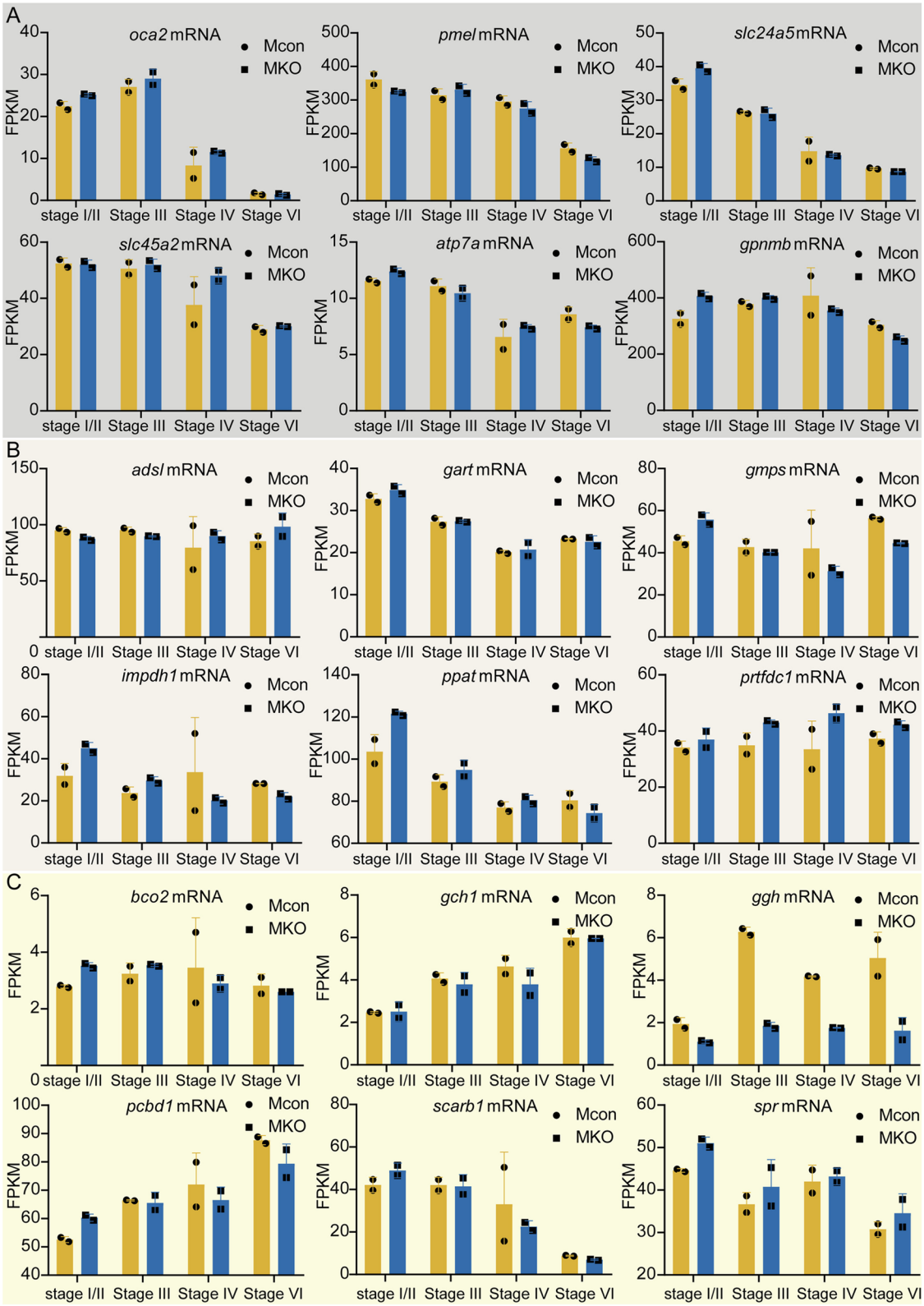

Fig. 5 (See legend on previous page.)

Other significant molecular features during oocyte development in *Xenopus tropicalis*

Transcriptome data from WT and *mitf*$^{-/-}$ *Xenopus tropicalis* oocytes were further analyzed to delineate key molecular features during oocyte development. Genes were selected based on a screening criterion of P value ≤ 0.05 and FPKM ≥ 1, with log2FC ranked in descending order, revealing that the top genes predominantly related to mitochondria (Additional file 2: Table S3). The expression patterns of these mitochondrial-related genes' mRNAs were consistent between WT and *mitf*$^{-/-}$ *Xenopus tropicalis* oocytes, showing no significant differences between the two groups (Fig. 6A–B and Additional file 2: Table S3). Specifically, expression levels were low during stages 1 and 2, increased significantly by stage 3, peaked at stage 4, and although slightly reduced by stage 6, it remained relatively high. During the development of *Xenopus tropicalis* oocytes, the expression levels of four mitochondrial-related genes, *cox1*, *cox2*, *cox3*, and *nd3*, are notably high (Fig. 6A–B and Additional file 2: Table S3). Among the key genes regulating mitochondrial biogenesis and functional homeostasis, *mfn1*, *mfn2*, and *tfam* mRNA levels remain relatively high throughout all stages of *Xenopus tropicalis* oocyte development (Fig. 6C–D and Additional file 2: Table S3). These findings indicate that extensive mitochondrial biogenesis is crucial for oocyte development in *Xenopus tropicalis*. Additionally, the data suggest that the formation of the mitochondrial cloud in these oocytes is tightly regulated by a genetic network [37]. Further elucidation of the mechanisms and roles of mitochondrial cloud formation during oocyte development is therefore of significant importance [37, 38].

The formation of the mitochondrial cloud is a significant feature during oocyte development, alongside the notable formation of the zona pellucida [39]. The zona pellucida is a transparent, tough, and light-permeable membrane surrounding the oocyte, primarily composed of several glycoproteins forming a clear extracellular matrix [40]. This structure encases the oocyte, playing crucial roles in protection, fertilization regulation, and embryo development. The main components of the zona pellucida are glycoproteins, including ZP1, ZP2, ZP3, and ZP4 [39, 40]. We examined the expression of homologous genes *zp2*, *zp3.2*, *zp4*, and *zp4.2* during *Xenopus tropicalis* oogenesis. The results showed that although the mRNA levels of *zp2*, *zp3.2*, and *zp4.2* slightly decreased as oocyte development progressed, they remained relatively low without significant changes (Fig. 6E–J and Additional file 2: Table S3). In contrast, the expression of *zp4* mRNA remained high throughout oogenesis but significantly decreased, particularly from stage 4 to stage 6 (Fig. 6E–J). Typically, the mRNAs of *zp2*, *zp3.2*, *zp4*, and *zp4.2* are transcribed in follicular cells, translated into corresponding proteins, and subsequently secreted around the oocyte to contribute to the formation of the zona pellucida [39–41]. However, our transcriptome sequencing detected a substantial presence of *zp2*, *zp3.2*, *zp4*, and *zp4.2* transcripts within the oocyte itself (Fig. 6E–J), indicating that the oocyte might also express these mRNAs during oogenesis. This finding warrants further experimental validation. Particularly, the changes in *zp4* mRNA expression and its relationship with the acrosome reaction merit further investigation [39, 42].

We examined the expression of genes associated with acentriolar spindle assembly during meiosis. The mRNA levels of *pcnt* and *tacc3* increased progressively during oogenesis, with *tacc3* mRNA showing relatively high levels (Fig. 6K–L and Additional file 2: Table S3). Pericentrin (PCNT) plays a crucial role in oocyte meiosis, being involved in the localization of acentriolar microtubule-organizing centers (aMTOCs), spindle assembly, and chromosome segregation [43]. TACC3 is essential for the localization and function of aMTOCs during meiosis. It promotes microtubule nucleation and stability by interacting with microtubule-associated proteins such as chTOG [43, 44]. In *Xenopus tropicalis*, the increasing expression levels of *pcnt* and *tacc3* mRNA during oogenesis suggest that these genes might play a regulatory role in meiosis.

Analysis of transcriptome data from WT and *mitf*$^{-/-}$ *Xenopus tropicalis* oocytes reveals that the molecular characteristics associated with mitochondrial cloud formation are the most prominent during oocyte development. This finding suggests that the mitochondrial cloud is crucial for oocyte maturation. Similar subcellular structures have been observed in the oocytes of various vertebrates, including humans, mice, and zebrafish, indicating evolutionary conservation [37, 38]. Thus, the *Xenopus tropicalis* mitochondrial cloud serves as an excellent model for studying its role and mechanisms in oocyte development. Furthermore, the expression patterns of zona pellucida proteins (*zp2*, *zp3.2*, *zp4*, and *zp4.2*) and meiosis-related genes (*pcnt* and *tacc3*) underscore the need to investigate their roles in oocyte development. Therefore, using *Xenopus tropicalis* as a model organism to study oogenesis is crucial for understanding reproductive biology.

Discussions

The potential off-target effects, particularly regarding the upregulation of other MIT family members such as Tfeb and Tfec, are a concern. Both factors are involved in cellular stress responses and may have compensatory roles in melanogenesis. Given their functional overlap with MITF, their roles in melanogenesis are highly relevant,

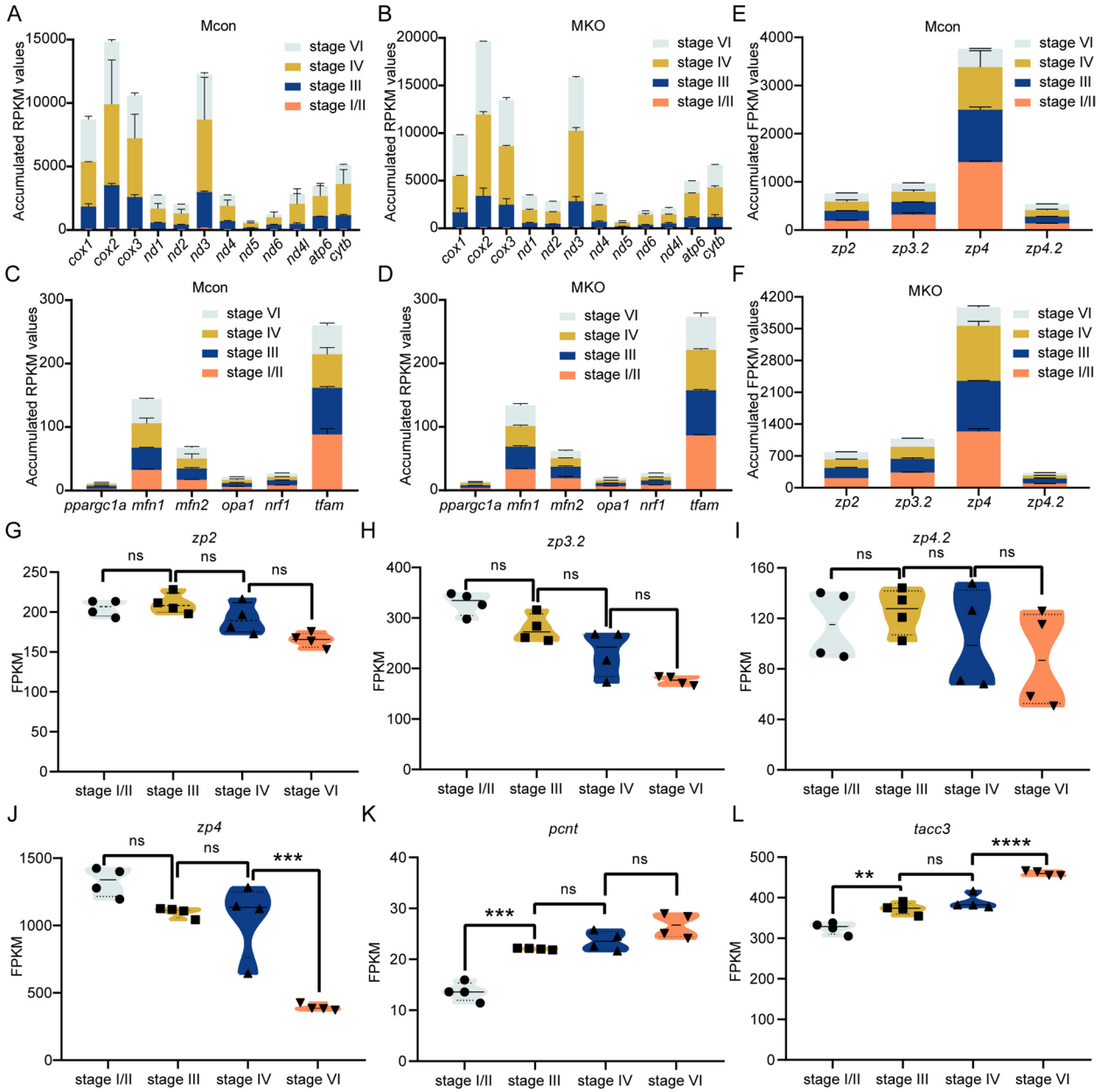

Fig. 6 Differentially expressed genes during oogenesis development in *Xenopus tropicalis*. **A** Expression of mitochondria-related genes during oogenesis in WT *Xenopus tropicalis*. **B** Expression of mitochondria-related genes during oogenesis in *mitf*$^{-/-}$ *Xenopus tropicalis*. **C** Expression of key genes regulating mitochondrial biogenesis during oogenesis in WT *Xenopus tropicalis*. **D** Expression of key genes regulating mitochondrial biogenesis during oogenesis in *mitf*$^{-/-}$ *Xenopus tropicalis*. **E** Expression of zona pellucida formation-related genes during oogenesis in WT *Xenopus tropicalis*. **F** Expression of zona pellucida formation-related genes during oogenesis in *mitf*$^{-/-}$ *Xenopus tropicalis*. **G–J** Average expression of zona pellucida formation-related genes *zp2*, *zp3.2*, *zp4.2*, and *zp4* during oogenesis in WT and *mitf*$^{-/-}$ *Xenopus tropicalis*. **K–L** Average expression of meiosis-related genes *pcnt* and *tacc3* during oogenesis in WT and *mitf*$^{-/-}$ *Xenopus tropicalis*. Results are shown as FPKM values. For **A–F**, the statistical tests are the Wald test and the Likelihood ratio test in Deseq2. For **G–L**, the statistical tests are the one-way ANOVA

especially since they regulate metabolic pathways and cellular homeostasis, which are essential for pigment cell function. However, we argue that off-target effects are unlikely to explain the observed melanogenesis in *mitf*$^{-/-}$ oocytes for three reasons: first, preliminary analysis suggests that off-target effects are improbable [26]. Second, there are no significant differences in the expression levels of *mitf*, *tfe3*, *tfec*, and *tfeb* mRNA between *mitf*$^{-/-}$ and wild-type oocytes (Fig. 3L–O and Additional file 1: Fig. S6A), indicating that any off-target effects did not

lead to changes in mRNA or protein expression. Third, the melanogenesis phenotype in *mitf*$^{-/-}$ oocytes has been observed across multiple generations (F1, F2, and F3) of *mitf*$^{-/-}$ *Xenopus tropicalis*, suggesting that any potential off-target effects are likely eliminated after multiple rounds of meiosis in germ cells with the *mitf*$^{-/-}$ genotype. Therefore, off-target effects are unlikely to account for the melanogenesis phenotype in *mitf*$^{-/-}$ oocytes, although further investigation is needed to definitively rule out this possibility.

In vertebrates, melanocyte development is conserved and originates from neural crest cells. However, skin pigment cell types vary significantly across taxa. Mammalian skin contains only melanocytes, which produce eumelanin and pheomelanin, whereas fish and amphibians have additional pigment cells, such as xanthophores and iridophores [45]. Even melanocytes, despite their conserved developmental pathways, exhibit species-specific differences in melanin synthesis [11]. Melanin synthesis occurs in melanosomes and produces eumelanin and pheomelanin. It begins with tyrosine, transported into melanocytes via membrane transporters, where TYR, the rate-limiting enzyme, oxidizes it to DOPA and then to dopaquinone [11]. Dopaquinone serves as a branching point [11]. Without sulfur-containing compounds, dopaquinone converts to dopachrome, which is processed by dopachrome tautomerase (DCT) into 5,6-dihydroxyindole (DHI) or 5,6-dihydroxyindole-2-carboxylic acid (DHICA). These intermediates are oxidized by TYRP1 and polymerized into eumelanin. In the presence of sulfur-containing amino acids, such as cysteine or glutathione, dopaquinone forms cysteinyldopa, which is oxidized into pheomelanin. Eumelanin, dark brown to black, provides strong UV absorption, antioxidant properties, and chemical stability [11]. Pheomelanin, yellow to red-brown, has weaker UV absorption and generates free radicals more readily [11]. Both types originate from tyrosine but diverge at dopaquinone through distinct pathways. Mammalian melanocytes produce both eumelanin and pheomelanin, while melanocytes in species like *Xenopus tropicalis* and zebrafish primarily produce eumelanin [11, 46].

Our study demonstrated that *mitf*$^{-/-}$ *Xenopus embryos* lack melanocytes from embryonic stage 33/34 to adulthood, except for black pigment in the ovarian peritoneum, nail regions, and retinal pigment epithelial cells [26]. Notably, rescuing *mitf* expression restores melanocyte development (Additional file 1: Fig.S8). Furthermore, melanocyte-related genes in the skin, such as *tyr*, *dct*, *pmel*, and *tyrp1*, were significantly downregulated in *mitf*$^{-/-}$ frogs, supporting the conserved role of Mitf in melanocyte regulation across vertebrates. Evidence shows that *Xenopus* oocyte pigmentation depends on Tyr function, as *tyr*$^{-/-}$ oocytes lack pigment. However, whether oocyte pigmentation relies on Mitf remains unclear. Several observations challenge the role of Mitf in oocyte pigmentation. First, although we constructed a *mitf*$^{-/-}$ *Xenopus* line, such models are rare in other species. Second, while *mitf*$^{-/-}$ frogs lack melanocytes, their oocytes retain pigmentation, and the expression of pigmentation-related genes (*tyr*, *dct*, *pmel*, *tyrp1*) remains unchanged compared to wild-type oocytes. This raises the question: which transcription factor regulates these genes in *mitf*$^{-/-}$ oocytes to drive pigmentation? Bioinformatics analysis and dual-luciferase assays suggest that Mitf, Tfe3, and Tfec regulate *tyr* and *dct* expression (Fig. 4 and Additional file 1: Fig.S7 and Additional file 3: Supplementary Note). Among these, only Tfe3 mRNA is highly expressed in both wild-type and *mitf*$^{-/-}$ oocytes, reaching levels comparable to *tyr* mRNA and surpassing the expression of other MiT family members by hundreds to thousands of times. These findings suggest that oocyte pigmentation in *Xenopus tropicalis* is independent of Mitf and likely regulated by Tfe3.

The MiT family, a group of bHLH-Zip transcription factors, primarily includes MITF, TFEB, TFEC, and TFE3 [14, 47]. These transcription factors typically bind to E-box sequences (CANNTG) via their bHLH-Zip domain to regulate target gene transcription. They can form homodimers (e.g., MITF-MITF) or heterodimers (e.g., MITF-TFEB), enhancing their DNA-binding ability and specificity [14, 47]. Consequently, they play crucial roles in gene expression, cell differentiation, metabolism, and autophagy. Tfec plays a direct role in regulating zebrafish iridophore development starting from the multipotent pigment cell progenitor stage [48]. It is also essential for iridophore development in a lizard model [49]. Therefore, it is hypothesized that Tfec regulates melanocyte development by influencing the differentiation of multipotent pigment cell progenitors, thereby affecting melanogenesis.

Although TFEB shares conserved domains with MITF, few studies report its direct role in melanogenesis [50, 51]. However, TFEB may influence melanogenesis indirectly through autophagy and lysosomal biogenesis [51]. Research shows that MITF-induced UVRAG expression is essential for UV-induced tanning, while TFEB or TFE3 inactivation has little effect on UVRAG expression after α-MSH stimulation [52]. This suggests TFEB and TFE3 do not regulate melanogenesis via the α-MSH pathway but underscores UVRAG's involvement in melanogenesis. UVRAG, a multifunctional protein critical for autophagy, endocytosis, and DNA damage repair, plays a central role in the Beclin1-VPS34 complex, which supports autophagosome formation and maturation [53]. While UVRAG's role in autophagy is well-established,

its connection to melanogenesis—via melanosome biogenesis and maturation—requires further exploration. UVRAG is vital for maintaining BLOC-1 complex stability, facilitating melanogenic cargo sorting [52]. Through interactions with the class C Vps complex, UVRAG activates RAB7 GTPase, promoting autophagosome–lysosome fusion, endosome–endosome fusion, and defective melanosome turnover, thereby indirectly affecting pigmentation [53]. For example, UVRAG-mediated autophagy may regulate melanogenic enzymes like tyrosinase or melanosome stability, influencing melanin synthesis. TFEB and TFE3, MiT/TFE transcription factors, are critical regulators of lysosomal biogenesis and autophagy, activating genes linked to these processes under nutrient deprivation or stress [51, 54]. While their direct role in melanogenesis remains unclear, they likely influence pigmentation by modulating UVRAG expression or its interactions with the class C Vps complex, affecting BLOC-1 stability and cargo trafficking. Notably, MITF induces UVRAG expression during UV-induced tanning, whereas TFEB or TFE3 inactivation has limited effect on UVRAG expression under α-MSH stimulation, further supporting their indirect involvement in melanogenesis [52]. Additionally, TFEB and TFE3 may regulate oxidative stress response genes, altering the redox balance in oocytes and indirectly influencing melanin synthesis [55, 56]. Future research should explore how UVRAG regulates autophagic flux and melanosome pathways in oocytes, identify upstream signals activating TFEB/TFE3 and their downstream autophagy-related targets, and investigate whether TFEB/TFE3 directly control melanogenic enzymes or UVRAG-mediated lysosomal activity. These studies will illuminate the links between autophagy, lysosomal biogenesis, and pigmentation, advancing our understanding of oocyte physiology and cellular mechanisms.

Although TFE3 cannot regulate melanogenesis via the α-MSH signaling pathway [52], Tfe3a can restore melanophore development at a very low frequency in zebrafish [57]. Additionally, TFE3 interacts with p300, further participating in melanogenesis-related signaling pathways [58]. Studies have shown that Tfe3 can activate the expression of Tyr and Tyrp1 [59]. Therefore, overall, although Tfeb, Tfec, and Tfe3 may be involved in the regulation of oocyte melanogenesis, considering that Tfe3 has a higher expression level in *Xenopus tropicalis* oocytes compared to the very low levels of Tfeb and Tfec, and considering the evidence that Tfe3 regulates Tyr and Tyrp1 expression, we hypothesize that Tfe3, rather than Mitf, regulates melanogenesis-related gene expression during oogenesis in *Xenopus tropicalis*. This regulation results in melanin deposition at the animal pole of the oocyte. Further experimental data elucidating the molecular mechanisms of melanin deposition in *Xenopus tropicalis* oocytes will enhance research in oogenesis and reproductive medicine.

Melanin synthesis is a complex and tightly regulated process involving key enzymes, such as tyrosinase, and modulation by signaling pathways and molecular mechanisms [9, 11]. The melanogenesis mechanisms in *Xenopus tropicalis* resemble those in other vertebrates, but species-specific differences, particularly in the MIT family members. In mammals, birds, amphibians, and fish, the general framework of melanogenesis is conserved, but the functional roles of MIT family members differ. In mammals, MITF regulates melanocyte development and function, affecting both melanocyte survival and melanin synthesis. In birds, MITF regulates feather patterning, including iridescence, which is less relevant in mammals. Unlike the relatively static pigmentation in mammals, *Xenopus tropicalis* and fish are more sensitive to environmental factors, with their melanogenesis mechanisms responding quickly to light and temperature changes. While MITF is a well-established regulator of melanogenesis in mammals, in *Xenopus tropicalis*, both Mitf and other MIT family members, such as Tfeb and Tfec, may have overlapping or distinct roles in regulating pigmentation, depending on species-specific cellular contexts. Understanding these differences provides insights into the evolution of pigmentation and the functional diversity of transcription factors like MITF across species.

The Wnt and MAPK signaling pathways, along with non-coding RNAs (ncRNAs), are critical regulators [9, 11, 12, 45]. ncRNAs, including microRNAs (miRNAs), long non-coding RNAs (lncRNAs), and circular RNAs (circRNAs), further fine-tune melanogenesis. miRNAs bind to the 3'-UTRs of target mRNAs, regulating translation or degradation [60, 61]. lncRNAs modulate gene expression and epigenetic changes, while circRNAs act as competitive endogenous RNAs (ceRNAs), sequestering miRNAs or directly influencing transcription and translation. Thus, the Wnt and MAPK pathways regulate MiT/TFE transcription factors and its downstream targets, while ncRNAs refine these pathways, influencing melanogenesis. These mechanisms may also play a role in melanin synthesis in oocytes, requiring further investigation.

Transcriptomic data indicate that mitochondrial cloud formation is one of the distinctive features during oogenesis. The mitochondrial cloud is a crucial structure that regulates energy metabolism, mitochondrial dynamics, and signaling during oocyte maturation. It plays a key role in mitochondrial biogenesis, ATP (adenosine triphosphate) production, and the clearance of damaged mitochondria through mitophagy, all of which are essential for maintaining cellular energy balance during

oocyte maturation. Mitochondrial function, particularly ATP production and reactive oxygen species regulation, is linked to critical signaling pathways such as mTOR and MAPK, which control cell growth, metabolism, and development. For example, activation of the MAPK signaling pathway is vital for the completion of meiosis. Furthermore, the mitochondrial cloud interacts with the endoplasmic reticulum to modulate calcium signaling and regulate processes like protein synthesis and apoptosis. These pathways are especially important during oocyte maturation, as proper mitochondrial function and signaling are essential for successful fertilization and early embryonic development. Specifically, *cox1*, *cox2*, and *cox3* encode subunits 1, 2, and 3 of cytochrome c oxidase (complex IV), respectively [62]. Subunits 1 and 2 form the catalytic core of complex IV, with subunit 2 transferring electrons from cytochrome c to the active center of subunit 1 [62, 63]. Subunit 3, though not part of the catalytic core, stabilizes the structure and function of complex IV [62, 63]. Cytochrome c oxidase, located on the inner mitochondrial membrane, is the terminal enzyme of the mitochondrial electron transport chain. Its primary function is to catalyze the transfer of electrons from cytochrome c to oxygen, producing water and simultaneously pumping protons from the mitochondrial matrix into the intermembrane space [62, 63]. This creates a transmembrane electrochemical gradient (proton gradient) that drives ATP synthesis. The *nd3* gene encodes subunit 3 of NADH dehydrogenase (complex I), the first complex in the mitochondrial electron transport chain [64]. Complex I transfers hydrogen atoms and electrons from NADH to coenzyme Q on the inner mitochondrial membrane [64]. This process also involves the pumping of protons from the mitochondrial matrix into the intermembrane space, contributing to the proton gradient for ATP synthesis [64]. Therefore, during development to stage 3, *Xenopus tropicalis* oocytes undergo extensive mitochondrial biogenesis and ATP production, indicating a high demand for energy as they progress from stage 3 to mature oocytes. In vertebrates, the mitochondrial cloud (Balbiani body) is essential for oocyte development, although its precise functions remain unclear. It likely supports energy metabolism by aggregating mitochondria to ensure their proper distribution and ATP production during oogenesis, enabling chromatin remodeling, cytoskeletal reorganization, and organelle biogenesis. The cloud also contributes to cell signaling, regulating calcium homeostasis, ROS signaling, and pathways such as AMPK (adenosine 5'-monophosphate-activated protein kinase) and mTOR. Its assembly may localize key signaling events for oocyte polarization, germ plasm localization, and follicular communication. Future research could utilize advanced imaging techniques (e.g., live-cell or super-resolution microscopy) and mitochondrial assays to investigate its dynamics. Omics approaches, including transcriptomics and proteomics, may identify signaling molecules or enzymes enriched in the cloud. Functional studies in model organisms (e.g., frogs, zebrafish, mice) could determine how disrupting cloud formation, through genetic knockouts or pharmacological inhibitors, impacts oocyte quality and development. Clinically, mitochondrial dysfunction in the cloud may contribute to oocyte aging, infertility, or impaired embryonic development. Therapies targeting mitochondrial function or reducing ROS damage could enhance outcomes in assisted reproduction.

Transcriptomic data also indicate that zona pellucida (ZP) proteins exhibit specific expression patterns during oogenesis, likely preparing for fertilization. Homology analysis of ZP proteins between humans and *Xenopus tropicalis* shows high conservation (Additional file 1: Fig. S9-12), suggesting that studying *Xenopus tropicalis* ZP proteins may provide insights into human reproductive biology. The ZP primarily comprises three to four glycoproteins (ZP1, ZP2, ZP3, and ZP4 in certain species), each playing crucial roles in oocyte maturation and fertilization [39–41]. ZP1 crosslinks ZP2 and ZP3, forming a stable three-dimensional network that ensures structural integrity. ZP2 facilitates sperm binding, enabling species-specific attachment before fertilization and preventing polyspermy through ovastacin-mediated degradation post-fertilization. ZP3 mediates initial sperm recognition, binding, and acrosome reaction induction via species-specific oligosaccharides interacting with sperm receptors like ADAM proteins and β−1,4-galactosyltransferase. ZP4, functionally overlapping with ZP3, enhances sperm binding and selectively filters sperm by interacting with acrosomal receptors [39–41]. Collectively, ZP proteins ensure species specificity, structural integrity, and embryo development. However, research on *Xenopus tropicalis* ZP proteins remains limited. Further studies could deepen our understanding of reproductive biology and inform treatments for human infertility.

Conclusions

Here, we provide evidence that pigment deposition in *Xenopus tropicalis* oocytes is independent of the master melanocyte regulator Mitf. $mitf^{-/-}$ frogs, which lack melanocytes, exhibit significantly reduced expression of key melanogenesis genes, indicating a loss of Mitf activity. However, $mitf^{-/-}$ oocytes still express *tyr* mRNA, enabling melanogenesis and melanin deposition at the animal pole. In contrast, $tyr^{-/-}$ oocytes lack melanin deposition, confirming the essential role of Tyr. Thus, *Xenopus tropicalis* oocyte melanogenesis occurs independently of

Mitf, likely regulated by other MiT subfamily members controlling the expression of *tyr*, *dct*, and *tyrp1* during oogenesis. Additionally, mitochondrial cloud formation represents a major molecular event in oocyte development, along with the expression of zona pellucida proteins and meiosis-related genes such as *pcnt* and *tacc3*. These findings suggest that further elucidation of the Tyr-dependent, Mitf-independent mechanisms of animal pole pigmentation will advance our understanding of melanogenesis and oocyte development. Moreover, *Xenopus tropicalis* oocytes provide a valuable model for studying the mitochondrial cloud, zona pellucida, meiosis, oogenesis, and reproductive medicine.

Methods

Xenopus tropicalis maintenance and husbandry

Adult *Xenopus tropicalis* frogs were obtained from Nasco (Fort Atkinson, WI, USA; http://www.enasco.com). The maintenance and husbandry of the frogs, as well as the procurement of their oocytes, adhered to established methods [26, 65]. All experiments involving *Xenopus tropicalis* were approved by the Institutional Animal Care and Use Committee of the Southern University of Science and Technology.

The procurement of *Xenopus tropicalis* oocytes

The establishment of $mitf^{-/-}$ and $tyr^{-/-}$ *Xenopus tropicalis* lines has been reported in our previous studies [26]. The method for collecting oocytes from WT, $mitf^{-/-}$, and $tyr^{-/-}$ *Xenopus tropicalis* was slightly modified from the protocol described in the literature [66]. First, healthy adult WT, $mitf^{-/-}$, and $tyr^{-/-}$ *Xenopus tropicalis* were selected. To reduce stress, the frogs were anesthetized with 0.2% MS-222 (tricaine methanesulfonate) before the procedure. The abdomen was disinfected with 70% ethanol, and a small incision (approximately 1–2 cm) was made in the center of the abdomen, taking care not to cut too deeply to avoid damaging internal organs. The ovaries were carefully removed through the incision, and a portion of the ovarian tissue was gently excised using scissors or forceps. The excised ovarian tissue was placed in a dish containing cold 1×MBS (modified Barth's saline for *Xenopus*) solution to prevent damage to the oocytes. The ovarian tissue was then repeatedly washed in 1×MBS solution to remove blood and debris. After washing, the ovarian tissue was transferred to 1×MBS solution containing 1.5 mg/mL collagenase and incubated at 25 °C for 1–5 h with gentle agitation to facilitate the release of oocytes from the ovarian tissue. The process was monitored under a stereomicroscope to ensure that the follicle cells were completely separated from the oocytes. Following incubation, the oocytes were washed multiple times with fresh 1×MBS solution to remove residual collagenase and debris. The oocytes were then observed under a stereomicroscope, and oocytes at various developmental stages were selected.

Dual luciferase assay

Seed 293 T cells at 150,000 cells per well in a 24-well plate. After 12 h, transfect the cells with the PGL3 plasmid (firefly luciferase) and the Renilla luciferase control plasmid using appropriate transfection reagents. Forty-eight hours post-transfection, collect cell samples for luciferase activity measurement. Discard the supernatant and add a suitable lysis buffer, incubating on ice for 10 min. Transfer 20 μL of the lysate to a new well for the assay. Prepare luciferase reaction solutions by diluting firefly luciferase substrate (50×) and Renilla luciferase substrate (50×) with their respective buffers to 1×working solutions. Allow the solutions to equilibrate to room temperature. Add 100 μL of the firefly luciferase reaction solution to the lysate, mix gently, and measure firefly luciferase activity using a luminometer. Then, add 100 μL of the Renilla luciferase reaction solution, mix gently, and measure Renilla luciferase activity. Samples were analyzed using the Yisheng Bio (11402ES60) kit. Protein sequences for Mitf, Tfe3, and Tfec in *Xenopus tropicalis* were obtained from the Uniprot database and DNA sequences from the NCBI database. The promoters of tyr and dct in *Xenopus tropicalis* are located 2000 bp upstream of the translation start site (TSS).

RNA-seq library preparation and RNA-seq analysis

Oocytes were collected from WT and $mitf^{-/-}$ adult frogs, with each group comprising two replicates. Oocytes were disrupted using a disposable syringe until completely lysed, and total RNA was extracted following the manufacturer's instructions for the TransZol Up lysis reagent (ET111-01, TransGen Biotech). The extracted RNA samples were submitted to Novogene for RNA-seq library preparation and sequencing. RNA-seq analysis was conducted by Wuhan Frasergen Information Co., Ltd. The previously published protocol guided the RNA-seq data analysis [67]. Briefly, SOAPnuke software (v2.1.0) was used to filter raw reads to obtain clean reads. Clean reads were aligned to the *Xenopus tropicalis* reference genome UCB_Xtro_10.0 using HISAT2 (https://www.ncbi.nlm.nih.gov/datasets/genome/GCF_000004195.4/). Bowtie2 software then mapped the quality-controlled sequences to the reference transcriptome. RSEM analyzed the Bowtie2 alignment results to determine the number of reads mapped to each transcript and calculate FPKM (fragments per kilobase per million bases) values. Differential expression analysis was performed using DESeq2. RNA-seq data has been publicly deposited to Genome

Sequence Archive (https://ngdc.cncb.ac.cn/gsa/) with the accession number CRA017994.

Hematoxylin–eosin staining, transmission electron microscopy (TEM)

The samples underwent histological analysis, starting with fixation in FAS eyeball fixative (Servicebio, Wuhan, China) at room temperature for 24 h. The fixed samples were then dehydrated using graded ethanol (75%, 85%, 95%, and 100%), followed by replacement with xylene and embedding in paraffin wax. Sections with a thickness of 6 μm were prepared from the embedded tissues and subsequently dewaxed in xylene. Rehydration was carried out using graded ethanol concentrations (100%, 95%, and 70%) before staining with the hematoxylin–eosin staining kit (Baso, Zhuhai, China) and immunofluorescent staining. Hematoxylin–eosin-stained results were captured using an Olympus BX53 upright microscope (Olympus, Japan).

Our previously published protocol guided the TEM sample preparation [26]. Briefly, *Xenopus tropicalis* tissue samples, sized 1 mm × 1 mm, were fixed overnight at 4 °C in 2% glutaraldehyde. Oocytes were also fixed overnight at 4 °C in 2% glutaraldehyde. For ovarian membrane black spot samples, the black spots were dissected under a stereomicroscope and processed as a single electron microscopy sample for each frog. For oocyte samples, 10 stage VI oocytes from a single frog were pooled and processed as one electron microscopy sample. Following fixation, the samples underwent four 10-min washes with 10 mM PBS solution. Subsequently, the samples were fixed with 1% osmium tetroxide at room temperature for 3 h. The samples were then washed twice with 10 mM PBS solution for 10 min each, followed by two washes with ddH_2O for 10 min each. After rinsing with ddH_2O, the samples were treated with a 2% uranyl acetate solution at room temperature for 2 h or overnight at 4 °C. Following this, the samples were washed four or more times with ddH_2O for 10 min each until the rinsed water was clear. Post-rinsing, the samples were dehydrated using a graded acetone series: 30% acetone once, 50% acetone once, 75% acetone once, and 100% acetone twice, each for 10 min. Simultaneously with the gradient dehydration, epoxy resin (9.8 g), dodecenyl succinic anhydride (5.6 g), N-methylhexylamine (4.6 g), and 2,4,6-tris(dimethylaminomethyl)phenol (0.28 mL) were thoroughly mixed at room temperature using a rotary mixer for at least 4 h to prepare a 100% resin mixture. Then, at room temperature, the samples were treated with 25% resin–acetone once, 50% resin–acetone once, 75% resin–acetone once, and 100% resin once, each for 1.5–2 h. Following these steps, new 100% resin was added, and the samples were left overnight at 4 °C. Unused 100% resin was sealed with parafilm and stored at 4 °C for later use. The next day, the samples were embedded in new 100% resin. Subsequently, the embedded samples were baked in a 60 °C oven for 2 days to complete the preparation of TEM samples for ultrathin sectioning. Finally, the prepared TEM samples were sent to Wuhan Servicebio Technology Co., Ltd. for ultrathin sectioning, TEM observation, and photography.

Abbreviations

UV	Ultraviolet
RPE	Retinal pigment epithelium
DOPA	Dihydroxyphenylalanine
MITF	Microphthalmia-associated transcription factor
TRP-1	Tyrosinase-related protein 1
TRP-2	Tyrosinase-related protein 2
PKA	Protein kinase A
MAPK	Mitogen-activated protein kinase
PTU	1-Phenyl 2-thiourea
TALEN	Transcription activator-like effector nuclease
CRISPR/Cas9	Clustered Regularly Interspaced Short Palindromic Repeats
bHLH-LZ	The basic helix-loop-helix leucine zipper
TADs	Transcription activation domains
NCBI	National Center for Biotechnology Information
WT	Wild type
TSS	Transcription start site
FPKM	Fragments per kilobase of exon model per million mapped fragments
log2FC	Log2 fold change
PCNT	Pericentrin
aMTOCs	Acentriolar microtubule-organizing centers
DCT	Dopachrome tautomerase
DHI	5,6-Dihydroxyindole
DHICA	5,6-Dihydroxyindole-2-carboxylic acid
ATP	Adenosine triphosphate
AMPK	Adenosine 5′-monophosphate-activated protein kinase
ZP	Zona pellucida
MBS	Modified Barth's Saline for Xenopus
MS-222	Tricaine methanesulfonate
TEM	Transmission electron microscopy

Supplementary Information

The online version contains supplementary material available at https://doi.org/10.1186/s12915-025-02168-0.

Additional file 1: Supplementary Figure S1-S9. Supplementary Figure S1. Transcripts of human *MITF* (A) and mouse *Mitf* (B). For detailed information, refer to NCBI. Supplementary Figure S2. In *mitf*$^{-/-}$ *Xenopus tropicalis*, the bHLHzip domain of the Mitf protein, is inactivated. A, the picture provides a schematic representation of the transcripts and related information of the *mitfa* gene locus in zebrafish and the *mitf* gene locus in *Xenopus tropicalis*. The red arrow indicates the penultimate exon, which is responsible for transcribing a common part of the transcripts from this gene locus. B and C, pictures display two different views of the 3D structure of the human MITF protein (encoded by transcript variant 4 of the human MITF gene locus, a master regulator of melanocyte development). The yellow-highlighted regions show the conserved amino acid sequences between the *Xenopus tropicalis* Mitf protein and the human MITF protein. The red arrow points to the knockout site in the *mitf*$^{-/-}$ *Xenopus tropicalis* Mitf protein. 'N' indicates the amino-terminal, and 'C' indicates the carboxy-terminal. D and E, the figure illustrate the amino acid sequence alignment of feature 1 (DNA binding site) and feature 2 (polypeptide binding site/dimer interface) of the bHLHzip domain among different vertebrate species. In D and E, red indicates high conservation and blue indicates low conservation. Hash-marks (#) in the top row of the multiple sequence alignment display indicate specific residues involved

in a conserved feature, such as a binding or catalytic site, that has been annotated on an NCBI-curated domain. The black arrows in A, D, and E indicate the knockout site of *mitf*$^{-/-}$ *Xenopus tropicalis mitf*. For detailed data analysis, refer to NCBI (https://www.ncbi.nlm.nih.gov/). Supplementary Figure S3. The transcriptomic comparison of dorsal (DS) and ventral (VS) skin samples from wild-type *Xenopus tropicalis* revealed significant overall differences in the expression of melanogenesis-related genes ($P = 0.0139$, paired t-test). Supplementary Figure S4. Differential expression of genes related to RPE cells and melanocytes in the eyes of WT and *mitf*$^{-/-}$ *Xenopus tropicalis*. Mcon denotes WT *Xenopus tropicalis* eye samples, while MKO denotes *mitf*$^{-/-}$ *Xenopus tropicalis* eye samples. Supplementary Figure S5. The number of black spots on the ovarian membrane was compared between adult WT and *mitf*$^{-/-}$ Xenopus tropicalis. Black spots were quantified within a 24 mm^2 area of the ovarian membrane using a stereomicroscope. Three frogs per genotype were analyzed, with two random areas sampled per frog. * indicates $P < 0.05$ (unpaired t-test). Supplementary Figure S6. A-C, Expression levels of *tfeb,tyrp1*, and *dct* mRNA during oocyte development in WT and *mitf*$^{-/-}$ Xenopus tropicalis. D, Comparison of amino acid sequences of human MITF-A, *Xenopus tropicalis* Mitf, and *Xenopus tropicalis* Tfe3 proteins. Protein sequence information was obtained from https://www.uniprot.org/. Supplementary Figure S7. The DNA motifs bound by MiT family transcription factors were derived from JASPAR (http://jaspar.genereg.net/). Panels A-B, C-D, E-F, and G-H display the nucleotide frequency and motif sequences at different positions for Tfe3, Mitf, Tfeb, and Tfec, respectively. Supplementary Figure S8. The dorsal views of adult WT, *mitf*-knockout (*mitf*$^{-/-}$), and *mitf*$^{-/-}$ rescue *Xenopus tropicalis* were compared. At least 100 frogs were analyzed for each group, except for the *mitf*$^{-/-}$ rescue. The scale bar represents 5 mm. Supplementary Figure S9-12. The homology of zona pellucida proteins between *Xenopus tropicalis* and human oocytes was compared using data from the UniProt database.

Additional file 2: Supplementary Table S1-S3. Supplementary Table S1. Gene expression profiles identified through bulk RNA-seq in the dorsal and ventral skin samples of WT (Mcon) and *mitf*$^{-/-}$ (MKO) *Xenopus tropicalis*. Supplementary Table S2. Gene expression profiles identified through bulk RNA-seq in the eye samples of wild-type WT (Mcon) and *mitf*$^{-/-}$ (MKO) *Xenopus tropicalis*. Supplementary Table S3. Gene expression profiles identified through bulk RNA-seq in the oocytes samples of wild-type WT (Mcon) and *mitf*$^{-/-}$ (MKO) *Xenopus tropicalis*.

Additional file 3: Supplementary Note. Transcription factor sequence information was obtained from the UniProt database, and DNA motif data were retrieved from the JASPAR database. The relevant results are presented in R-Table S1 to R-Table S4.

Acknowledgements
This work was supported by the Center for Computational Science and Engineering at Southern University of Science and Technology. We are also grateful to Professor Jiayin Shen for his professional guidance, which has been essential for the project's success. Finally, we thank the other members of our team for their contributions.

Authors' contributions
R.R. and H.L.2 (Hongzhou Lu) and Y.C. and W.L. conceived the project. H.Y. and W.L. and S.Y. performed the experiments and analyzed the data together with.H.L.1 (Han Liu) and J.D. and X.F.. S.H. and W.C. contributed TEM data collation and analysis. R.R. and H.Y. wrote the manuscript with input from all the authors. J.H. and H.L.2 and Y.C. revised the article. All authors contributed to discussions of the results and manuscript revision. All authors read and approved the final manuscript.

Funding
This work was supported by the National Natural Science Foundation of China (Nos. 32,300,659, 32,470,880), Shenzhen Science and Technology Innovation Commission Project (No. JCYJ20230807143302004), Shenzhen Clinical Research Center for Emerging Infectious Diseases (No. LCYSSQ20220823091203007), and Shenzhen High-level Hospital Construction Fund (No. XKJS-CRGRK-008, XKJS-CRGRK-011).

Data availability
RNA-seq data has been publicly deposited to Genome Sequence Archive (https://ngdc.cncb.ac.cn/gsa/) with the accession number CRA017994.

Declarations

Ethics approval and consent to participate
Not applicable.

Consent for publication
Not applicable.

Competing interests
The authors declare no competing interests.

Received: 26 July 2024 Accepted: 18 February 2025
Published online: 27 February 2025

References

1. Sánchez F, Smitz J: Molecular control of oogenesis. Biochimica et Biophysica Acta (BBA)-Molecular Basis of Disease 2012, 1822(12):1896–1912.
2. Salazar-Nicholls MJ, Hervas F, Muñoz-Tobar SI, Carrillo A-B, Ricaurte H, Ron SR, Romero-Carvajal A: A polymorphism in oocyte pigmentation in natural populations of the glass frog Espadarana prosoblepon (Centrolenidae). The International journal of developmental biology 2021, 65(4–5–6):333–344.
3. Harsa-King ML. Melanogenesis in oocytes of wild-type and mutant albino axolotls. Dev Biol. 1980;74(2):251–62.
4. Dumont JN. Oogenesis in Xenopus laevis (Daudin). I. Stages of oocyte development in laboratory maintained animals. Journal of morphology. 1972;136(2):153–79.
5. Dumont JN, Eppig JJ Jr. A method for the production of pigmentless eggs in Xenopus laevis. J Exp Zool. 1971;178(3):307–11.
6. Cajas YN, Cañón-Beltrán K. Ladrón de Guevara M, Millán de La Blanca MG, Ramos-Ibeas P, Gutiérrez-Adán A, Rizos D, González EM: Antioxidant nobiletin enhances oocyte maturation and subsequent embryo development and quality. Int J Mol Sci. 2020;21(15):5340.
7. Molina-Carrillo L, Bassaglia Y, Schires G, Bonnaud-Ponticelli L. Does the egg capsule protect against chronic UV-B radiation? A study based on encapsulated and decapsulated embryos of cuttlefish Sepia officinalis. Royal Society Open Science. 2023;10(7): 230602.
8. Wisocki PA, Kennelly P, Rojas Rivera I, Cassey P, Burkey ML, Hanley D. The global distribution of avian eggshell colours suggest a thermoregulatory benefit of darker pigmentation. Nature Ecology & Evolution. 2020;4(1):148–55.
9. Wakamatsu K, Ito S: Melanins in vertebrates. Pigments, pigment cells and pigment patterns 2021:45–89.
10. McNamara ME, Rossi V, Slater TS, Rogers CS, Ducrest A-L, Dubey S, Roulin A. Decoding the evolution of melanin in vertebrates. Trends Ecol Evol. 2021;36(5):430–43.
11. Liliana DA, Matthew DS. Melanosomes: biogenesis, properties, and evolution of an ancient organelle. Physiol Rev. 2018;99(1):1–19.
12. Marelize S, Rachel Elizabeth W, Sophia Nicole W, Jennifer Gibson G. The metabolism of melanin synthesis-from melanocytes to melanoma. Pigment Cell Melanoma Res. 2024;37(4):438–52.
13. D'Mello SA, Finlay GJ, Baguley BC, Askarian-Amiri ME. Signaling pathways in melanogenesis. Int J Mol Sci. 2016;17(7):1144.
14. Goding CR, Arnheiter H. MITF-the first 25 years. Genes Dev. 2019;33(15–16):983–1007.
15. Centeno P, Pavet V, Marais R. The journey from melanocytes to melanoma. Nat Rev Cancer. 2023;23(6):372–90.
16. Shihang Z, Hongliang Z, Jinhua H, Li L, Xiaoliang T, Si L, Ying Z, Haoran G, Manal K, Liping L, et al. Epigenetic regulation of melanogenesis. Ageing Res Rev. 2021;69(0):101349.

17. Yekatsiaryna H, Irene B, Lucia O-G, Giulia Di M, Fernanda M, Mauro T, Monica De M. microRNAs in the regulation of melanogenesis. Int J Mol Sci. 2021;22(11):6104.
18. Paleček J, Ubbels GA, Rzehak K. Changes of the external and internal pigment pattern upon fertilization in the egg of Xenopus laevis. Development. 1978;45(1):203–14.
19. Eppig JJ Jr, Dumont JN. The distribution of melanosomes in larvae reared from normal and from pigmentless eggs of Xenopus laevis. J Exp Zool. 1971;177(1):79–88.
20. Eppig JJ, Dumont JN. Oogenesis in Xenopus laevis (Daudin): II. The induction and subcellular localization of tyrosinase activity in developing oocytes. Developmental Biology. 1974;36(2):330–42.
21. Eppig Jr JJ: Melanogenesis in amphibians. III. The buoyant density of oocyte and larval Xenopus laevis melanosomes and the isolation of oocyte melanosomes from the eyes of PTU-treated larvae. Journal of Experimental Zoology 1970, 175(4):467–475.
22. Wyllie A, Robertis ED. High tyrosinase activity in albino Xenopus laevis oocytes. Development. 1976;36(3):555–9.
23. Merriam R, Sauterer R. Localization of a pigment-containing structure near the surface of Xenopus eggs which contracts in response to calcium. Development. 1983;76(1):51–65.
24. Kidson S, Fabian B. Synthesis and activity of Xenopus laevis oocyte tyrosinase. J Exp Zool. 1989;249(2):203–12.
25. Naert T, Van Nieuwenhuysen T, Vleminckx K: TALENs and CRISPR/Cas9 fuel genetically engineered clinically relevant Xenopus tropicalis tumor models. genesis 2017, 55(1–2):e23005.
26. Ran R, Li L, Xu T, Huang J, He H, Chen Y. Revealing mitf functions and visualizing allografted tumor metastasis in colorless and immunodeficient Xenopus tropicalis. Communications Biology. 2024;7(1):275.
27. Prospéri M-T, Giordano C, Gomez-Duro M, Hurbain I, Macé A-S, Raposo G, D'angelo G. Extracellular vesicles released by keratinocytes regulate melanosome maturation, melanocyte dendricity, and pigment transfer. Proc Natl Acad Sci. 2024;121(16): e2321323121.
28. Hernandez-Medrano J, Belmpa M: Folliculogenesis and oogenesis. In: Mastering Clinical Embryology. CRC Press; 2024: 75–81.
29. Vachtenheim J, Borovansky J. "Transcription physiology" of pigment formation in melanocytes: central role of MITF. Exp Dermatol. 2010;19(7):617–27.
30. Ma X, Li H, Chen Y, Yang J, Chen H, Arnheiter H, Hou L. The transcription factor MITF in RPE function and dysfunction. Prog Retin Eye Res. 2019;73: 100766.
31. Lee A, Lim J, Lim J-S: Emerging roles of MITF as a crucial regulator of immunity. Experimental & Molecular Medicine 2024:1–8.
32. Vachtenheim J, Drdová B. A dominant negative mutant of microphthalmia transcription factor (MITF) lacking two transactivation domains suppresses transcription mediated by wild type MITF and a hyperactive MITF derivative. Pigment Cell Res. 2004;17(1):43–50.
33. JJE, JND. Oogenesis in Xenopus laevis (Daudin). II. The induction and subcellular localization of tyrosinase activity in developing oocytes. Dev Biol. 1974;36(2):330–42.
34. SHK, BCF. Synthesis and activity of Xenopus laevis oocyte tyrosinase. J Exp Zool. 1989;249(2):203–12.
35. OAH. Induction - the main principle of melanogenesis in early development. Differentiation. 1981;20(2):104–16.
36. Rauluseviciute I, Riudavets-Puig R, Blanc-Mathieu R, Castro-Mondragon JA, Ferenc K, Kumar V, Lemma RB, Lucas J, Chèneby J, Baranasic D, et al. JASPAR 2024: 20th anniversary of the open-access database of transcription factor binding profiles. Nucleic Acids Res. 2024;52(D1):D174-d182.
37. FSB, EA. The structure of the mitochondrial cloud of Xenopus laevis oocytes. J Embryol Exp Morphol. 1976;36(3):697–710.
38. Malgorzata K, Szczepan B, Laurence DE. The Balbiani body and germ cell determinants: 150 years later. Curr Top Dev Biol. 2004;59(0):1–36.
39. Gupta SK. The human egg's zona pellucida. Curr Top Dev Biol. 2018;130:379–411.
40. Jovine L, Darie CC, Litscher ES, Wassarman PM. Zona pellucida domain proteins. Annu Rev Biochem. 2005;74:83–114.
41. Gupta SK. Zona pellucida glycoproteins: Relevance in fertility and development of contraceptive vaccines. Am J Reprod Immunol. 2023;89(2): e13535.
42. Litscher ES, Wassarman PM. Zona pellucida proteins, fibrils, and matrix. Annu Rev Biochem. 2020;89:695–715.
43. Wu T, Dong J, Fu J, Kuang Y, Chen B, Gu H, Luo Y, Gu R, Zhang M, Li W. The mechanism of acentrosomal spindle assembly in human oocytes. Science. 2022;378(6621):eabq7361.
44. Peset I, Vernos I. The TACC proteins: TACC-ling microtubule dynamics and centrosome function. Trends Cell Biol. 2008;18(8):379–88.
45. Junying Q, Mengjun Y, Yimeng F, Jing Z, Ting X, Fan L, Kun Z, Luqing H, Libo J, Da S. Zebrafish in dermatology: a comprehensive review of their role in investigating abnormal skin pigmentation mechanisms. Front Physiol. 2023;14(0):1296046.
46. Iain SH, Eric WR, Maria Luisa M, Katsutoshi Y, Hubert V, Jennifer EK, David MP, Paul FAM, Ralf P. From frog integument to human skin: dermatological perspectives from frog skin biology. Biol Rev Camb Philos Soc. 2013;89(3):618–55.
47. La Spina M, Contreras PS, Rissone A, Meena NK, Jeong E, Martina JA. MiT/TFE family of transcription factors: an evolutionary perspective. Frontiers in Cell and Developmental Biology. 2021;8: 609683.
48. Petratou K, Spencer SA, Kelsh RN, Lister JA. The MITF paralog tfec is required in neural crest development for fate specification of the iridophore lineage from a multipotent pigment cell progenitor. PLoS ONE. 2021;16(1): e0244794.
49. Garcia-Elfring A, Sabin CE, Iouchmanov AL, Roffey HL, Samudra SP, Alcala AJ, Osman RS, Lauderdale JD, Hendry AP, Menke DB. Piebaldism and chromatophore development in reptiles are linked to the tfec gene. Current Biology. 2023;33(4):755-763e753.
50. Napolitano G, Ballabio A. TFEB at a glance. J Cell Sci. 2016;129(13):2475–81.
51. Settembre C, Di Malta C, Polito VA, Arencibia MG, Vetrini F, Erdin S, Erdin SU, Huynh T, Medina D, Colella P. TFEB links autophagy to lysosomal biogenesis. Science. 2011;332(6036):1429–33.
52. Yang Y. Jang G-b, Yang X, Wang Q, He S, Li S, Quach C, Zhao S, Li F, Yuan Z: Central role of autophagic UVRAG in melanogenesis and the suntan response. Proc Natl Acad Sci. 2018;115(33):E7728–37.
53. Liang C. Lee J-s, Inn K-S, Gack MU, Li Q, Roberts EA, Vergne I, Deretic V, Feng P, Akazawa C: Beclin1-binding UVRAG targets the class C Vps complex to coordinate autophagosome maturation and endocytic trafficking. Nat Cell Biol. 2008;10(7):776–87.
54. Heidi M-S, Yin X, Andrea B, Hui Z. The autophagy-lysosomal pathway in neurodegeneration: a TFEB perspective. Trends Neurosci. 2016;39(4):221–34.
55. Raben N, Puertollano R. TFEB and TFE3: linking lysosomes to cellular adaptation to stress. Annu Rev Cell Dev Biol. 2016;32:255–78.
56. Martina JA, Diab HI, Brady OA, Puertollano R. TFEB and TFE3 are novel components of the integrated stress response. Embo j. 2016;35(5):479–95.
57. Lister JA, Close J, Raible DW. Duplicate mitf genes in zebrafish: complementary expression and conservation of melanogenic potential. Dev Biol. 2001;237(2):333–44.
58. Steingrímsson E, Copeland NG, Jenkins NA. Melanocytes and the microphthalmia transcription factor network. Annu Rev Genet. 2004;38:365–411.
59. Verastegui C, Bertolotto C, Bille K, Abbe P, Ortonne JP, Ballotti R. TFE3, a transcription factor homologous to microphthalmia, is a potential transcriptional activator of tyrosinase and Tyrpl genes. Mol Endocrinol. 2000;14(3):449–56.
60. Marco A, Grant NW. MicroRNAs in neural crest development and neurocristopathies. Biochem Soc Trans. 2022;50(2):965–74.
61. Katerina G, Ioannis G, Arin G, Vishaka G, Gulden O, Huaitian L, George C K, Ilias S, Sophia G, Constantinos S, et al. Noncoding RNA circuitry in melanoma onset, plasticity, and therapeutic response. Pharmacol Ther. 2023;248(0):108466.
62. Suleva P-C, Michele B, Erika F-V. Emerging mechanisms in the redox regulation of mitochondrial cytochrome c oxidase assembly and function. Biochem Soc Trans. 2024;52(2):873–85.
63. Alba T-G, Eva N, Luciano AA, Alejandro JV, Jonathan H, Antoni B. Mitochondrial cytochrome c oxidase biogenesis: recent developments. Semin Cell Dev Biol. 2017;76(0):163–78.
64. Sazanov LA. A giant molecular proton pump: structure and mechanism of respiratory complex I. Nat Rev Mol Cell Biol. 2015;16(6):375–88.
65. Ran R, Li L, Shi Z, Liu G, Jiang H, Fang L, Xu T, Huang J, Chen W, Chen Y. Disruption of tp53 leads to cutaneous nevus and melanoma formation in Xenopus tropicalis. Mol Oncol. 2022;16(19):3554–67.

66. Newman K, Aguero T, King ML: Isolation of Xenopus oocytes. Cold Spring Harbor Protocols 2018, 2018(2):pdb. prot095851.
67. Shi Z, Liu G, Jiang H, Shi S, Zhang X, Deng Y, Chen Y. Activation of P53 pathway contributes to Xenopus hybrid inviability. Proc Natl Acad Sci. 2023;120(21): e2303698120.

Publisher's Note